

# Propagation of Spindle Waves in a Thalamic Slice Model

DAVID GOLOMB, XIAO-JING WANG, AND JOHN RINZEL

Mathematical Research Branch, National Institute of Diabetes and Digestive and Kidney Diseases,  
National Institutes of Health, Bethesda, Maryland 20814; and Department of Mathematics, University of Pittsburgh,  
Pittsburgh, Pennsylvania 15260

## SUMMARY AND CONCLUSIONS

1. We study the propagation and dynamics of spindle waves in thalamic slices by developing and analyzing a model of reciprocally coupled populations of excitatory thalamocortical (TC) neurons and inhibitory thalamic reticular (RE) neurons.

2. Each TC neuron has three intrinsic ionic currents: a low-threshold T-type  $\text{Ca}^{2+}$  current ( $I_{\text{Ca-T}}$ ), a hyperpolarization-activated cation ("sag") current ( $I_h$ ), and a leak current. Each RE cell also has three currents:  $I_{\text{Ca-T}}$ , a leak current, and a calcium-activated potassium current ( $I_{\text{AHP}}$ ). Isolated TC cells are at rest, can burst when released or depolarized from a hyperpolarized level, and burst rhythmically under moderate constant hyperpolarizing current. Isolated RE cells are at a hyperpolarized resting membrane potential and can burst when depolarized.

3. TC cells excite RE cells with fast  $\alpha$ -amino-3-hydroxy-5-methyl-4-isoxazolepropionic acid (AMPA) synapses, and RE cells inhibit TC cells with fast  $\gamma$ -aminobutyric acid-A (GABA<sub>A</sub>) and slow GABA<sub>B</sub> synapses and inhibit each other with GABA<sub>A</sub> synapses only. GABA<sub>B</sub> postsynaptic conductances operate far from saturation, and the slow inhibitory postsynaptic potentials (IPSPs) increase with the width of the presynaptic burst. The model network is a one-dimensional cellular array with localized coupling. The synaptic coupling strength decays with the distance between the pre- and postsynaptic cells, either exponentially or as a step function.

4. The "intact" network can oscillate with partial synchrony and a population frequency of  $\sim 10$  Hz. RE cells emit bursts almost at every oscillation cycle, whereas TC cells do so almost at every other cycle. Block of GABA<sub>B</sub> receptors hardly changes the network behavior. Block of GABA<sub>A</sub> receptors leads the network to a slowed oscillatory state, where the population frequency is  $\sim 4$  Hz and both RE and TC cells fire unusually long bursts at every cycle and in full synchrony. These results are consistent with the experimental observations of von Krosigk, Bal, and McCormick. We obtain such consistency only when the above assumptions regarding the synaptic dynamics, particularly nonsaturating GABA<sub>B</sub> synapses, are fulfilled.

5. The slice model has a stable rest state with no neural activity. By initially depolarizing a few neurons at one end of the slice while all the other cells are at rest, a recruitment process may be initiated, and a wavefront of oscillatory activity propagates across the slice. Ahead of the wavefront, neurons are quiescent; neurons behind it oscillate. We find that the wave progresses forward in a lurching manner. TC cells that have just become inhibited must be hyperpolarized for a long enough time before they can fire rebound bursts and recruit RE cells. This step limits the wavefront velocity and may involve a substantial part of the cycle when no cells at the front are depolarized.

6. The wavefront velocity increases linearly with the characteristic spatial length of the connectivity (the footprint length). It increases only gradually with the synaptic strength, logarithmically in the case of an exponential connection function and only slightly for a step connection function. It also decreases gradually with a potassium leak conductance that hyperpolarizes RE cells.

7. To reproduce the experimentally measured wavefront velocity of  $\sim 1$  mm/s, together with other *in vitro* observations, both the RE-to-TC and the TC-to-RE projections in the model should be spatially localized. The sum of the RE-to-TC and the TC-to-RE synaptic footprint lengths should be on the order of  $100 \mu\text{m}$ .

8. Neurons at different positions along the slice model oscillate with different phases. In the case of GABA<sub>A</sub> blockade, the phase shifts increase linearly with the distance between neurons and decay only slowly with time. Depending on parameter values, the phase shift can be positive or negative, because in a given bursting cycle a neuron fires before or after those on its right side, respectively. With GABA<sub>A</sub> intact, the phase shift's dependence on interneuronal distance can fluctuate and be more complex.

9. In addition to a propagating wavefront, the network can display various other types of spatiotemporal behaviors as parameter values and initial conditions are varied. Even a few endogenously oscillating cells, as expected in a heterogeneous population, can lead to several initiation points for waves propagating in both directions. The isolated RE network can oscillate with partial synchrony if the RE cells are less hyperpolarized, similar to *in vivo* results on the isolated RE nucleus by Steriade and colleagues.

## INTRODUCTION

Among different types of collective neuronal oscillations observed in the brain (Gray 1994), the 7- to 14-Hz spindle rhythmicity is characterized by its spontaneous occurrence at the onset of sleep or drowsiness, and by a high degree of coherence throughout the entire thalamocortical system (Andersen and Andersson 1968; Buzsaki 1991; Steriade and Deschênes 1984; Steriade et al. 1990, 1993). It has been known since the 1940s that the thalamus is at the origin of this rhythmic phenomenon (Morison and Bassett 1945). Spindle rhythrogenesis involves principally two types of thalamic neurons: the thalamocortical (TC) relay cells excite the reticular thalamic (RE) cells, which in turn send back synaptic inhibition to TC cells and elicit postinhibitory rebound (PIR) bursts of action potentials in these cells (Steriade et al. 1985, 1990, 1993). The rebound response to inhibitory postsynaptic potentials (IPSPs) is produced by a low-threshold T-type  $\text{Ca}^{2+}$  current  $I_{\text{Ca-T}}$  (Deschênes et al. 1984; Jahnsen and Llinás 1984a,b; Pape et al. 1994), together with a hyperpolarization-activated cation "sag" current  $I_h$  (Leresche et al. 1991; McCormick and Pape 1990).

We have developed computational models of the thalamic circuit underlying the spindle oscillation genesis. In particular, we have explored the possibility, as suggested by the experimental data of Steriade and colleagues, that an isolated RE nucleus is capable of displaying population spindle oscillations (Steriade et al. 1987). The RE cells are intercon-

nected by GABAergic synapses (Steriade et al. 1990) and also exhibit PIR due to an intrinsic  $I_{Ca-T}$  current with somewhat slower kinetics than  $I_{Ca-T}$  in TC cells (Huguenard and Prince 1992). In our previous work on an RE network (Golomb and Rinzel 1993, 1994; Golomb et al. 1994a; Wang and Rinzel 1992, 1993), we analyzed how coherent oscillations can result from the interplay between the cellular PIR property and the synaptic inhibition in the RE network. The results from a globally connected network model (Golomb et al. 1994a), as well as those using a distance-dependent connectivity architecture (Destexhe et al. 1994a), suggest that an isolated RE nucleus may indeed be able to oscillate at spindle frequencies, although generally not in a fully synchronous fashion.

Subsequently, our model was extended to include a TC cell population, and the effects of reciprocal connections between TC and RE cell types were studied in a network with random connectivities (Wang et al. 1995); a two-cell TC-RE idealization was also considered by Destexhe et al. (1993). The hypothesis that spindle oscillations can emerge from the RE-TC two-way interactions has been suggested by various experimental studies and does not require (nor necessarily exclude under certain conditions) that the RE nucleus acts as an autonomous oscillator. This hypothesis received direct support from recent results on *in vitro* ferret thalamic slice preparations, which contain the dorsal lateral geniculate nucleus (LGN) in reciprocal connections with the perigeniculate nucleus (PGN) (Bal et al. 1994, 1995a,b; Kim et al. 1995; Lee et al. 1994; McCormick and Bal 1994; von Krosigk et al. 1993). These ferret slice experiments can be well controlled, and they provide systematic and detailed observations regarding the neuronal and synaptic mechanisms underlying spindle generation. We summarize here some of the main observations that are relevant to our work.

1. In intact slices (with no pharmacological manipulation of synaptic transmission), spontaneous as well as evoked spindle episodes occur with intraspindle burst frequency of 5–9 Hz. RE cells fire bursts almost at every cycle in coherence with the local population rhythm, but sometimes they skip bursts. TC cells fire bursts only at every two, three, or more cycles, but always phase locked with the local population rhythm.

2. The bursting pattern is hardly changed when  $\gamma$ -aminobutyric acid-B ( $GABA_B$ ) receptors are blocked with 2-hydroxysaclofen (25–1,000  $\mu M$ ).

3. When  $GABA_A$  receptors are blocked with bicuculline methiodide (20–50  $\mu M$ ), the population frequency is reduced to 2–4 Hz. Both RE and TC cells fire prolonged bursts at almost every cycle, with a dramatic decrease of burst skipping events. The population rhythm is highly synchronized.

4. When both  $GABA_A$  and  $GABA_B$  receptors are blocked, the network is quiescent.

5. When  $\alpha$ -amino-3-hydroxy-5-methyl-4-isoxazolepropionic acid (AMPA) receptors are blocked by 6-cyano-7-nitroquinoxaline-2,3-dione (CNQX; 250  $\mu M$ ), the network is quiescent.

6. Spindle episodes in the intact slice as well as in the presence of bicuculline appear as traveling fronts that propagate with a velocity around 1 mm/s.

A model of spatiotemporal behaviors of spindling thala-

mic slices should be consistent with the known cellular and synaptic biophysical properties of the thalamus and able to reproduce all the above observations. Its goal is to illuminate the role of intrinsic ionic channels, synaptic coupling and architecture in the generation of spindle rhythmicity in particular, and collective neural dynamical behavior in general. In the thalamic model of Wang et al. (1995), coherent oscillations at the spindle frequencies were generated by the reciprocal interactions between TC and RE cell populations. Using a network with random and sparse connectivity, we reproduced the first five results of the slice experiment (the 6th one is irrelevant for a model without geometry). However, when the  $GABA_A$  receptors were blocked, the slowed synchronous oscillation in the model was somewhat fragile because it coexisted with an asynchronous state that had a sizeable domain of attraction. We studied the effects of the RE-TC convergence/divergence factors and showed that a small number of inputs per cell, say <10, is generally enough for maintaining a high degree of network synchrony. The burst skipping phenomenon in TC cells was explained in terms of a temporal integration of rhythmic IPSPs by the slow inward current  $I_h$  and was shown to be more pronounced when TC cells were more hyperpolarized.

The objective of the present work is to improve upon that RE-TC network model in two important ways. First, this network model has a spatially dependent connection architecture, so the main focus of this paper will be on the wave propagation of spindle episodes across the “model slice.” Second, we introduce a new phenomenological model for the  $GABA_B$  synapses, so that the postsynaptic conductance operates far from saturation and amplifies nonlinearly as a function of the presynaptic RE burst width. With this model, we can account for the experimental *results 1–6* in a robust manner. In particular, we have found a new type of wavefront that advances in a lurching manner. Macroscopic groups of TC and RE cells are recruited discontinuously; once each oscillation cycle, new groups of TC and RE cells join the population rhythm. The dependence of the wavefront velocity on the characteristic spatial lengths of TC-RE connections and on other model parameters is investigated in detail.

A preliminary report of the present work was published in abstract form (Golomb et al. 1994b).

## METHODS

### *Single-cell models*

The single-cell models have only one compartment and are represented by coupled differential equations according to the Hodgkin-Huxley-type scheme, similar to our previous works (Golomb et al. 1994a; Wang et al. 1995). Sodium spike-generating currents are not included for simplicity. The equations and parameters of the model neurons are given in APPENDIX A.

### *RE CELL*

$$C \frac{dV}{dt} = -I_{Ca-T} - I_{AHP} - I_{KL} - I_{NL} - I_{GABA_A}^{RR} - I_{AMPA} \quad (1)$$

where  $I_{Ca-T}$  is the low-threshold calcium current,  $I_{AHP}$  is a calcium-activated potassium current, and  $I_{KL}$  and  $I_{NL}$  are the potassium and nonspecific leak currents, respectively.

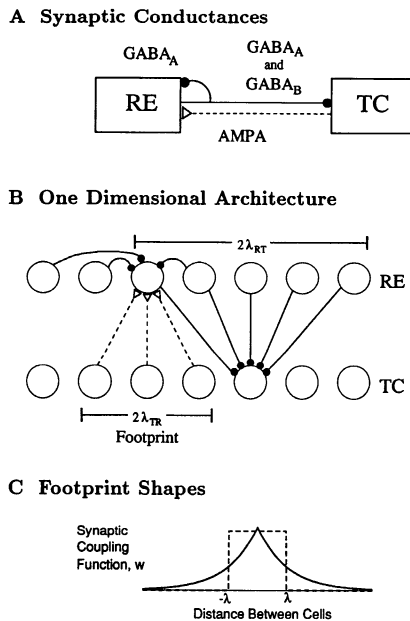


FIG. 1. Synaptic architecture of the model. *A*: reticular (RE) cells receive thalamocortical (TC) excitation via  $\alpha$ -amino-3-hydroxy-5-methyl-4-isoxazolepropionic acid (AMPA) synapses and intra-RE inhibition via  $\gamma$ -aminobutyric acid-A (GABA<sub>A</sub>) synapses. TC cells receive both fast GABA<sub>A</sub> and slow GABA<sub>B</sub> synapses from RE cells. *B*: the model has a 1-dimensional architecture. The RE-to-TC coupling strength (maximal synaptic conductance) decays with the distance between the pre- and postsynaptic cells. The typical decay length,  $\lambda_{TR}$ , is called the synaptic footprint length. Similarly, the TC-to-RE coupling strength decays with a typical length  $\lambda_{TR}$ , and the RE-to-RE coupling strength with a typical length  $\lambda_{RR}$  (not shown). *C*: for an exponential footprint shape (—) the typical decay length  $\lambda$  (which is either  $\lambda_{RT}$ ,  $\lambda_{TR}$ , or  $\lambda_{RR}$ ) is the spatial distance for which the coupling strength reaches  $1/e$  of its maximal value. For a step footprint shape (---), the coupling strength has a constant value if the interneuronal distance is between  $-\lambda$  and  $\lambda$ , and it is 0 otherwise.

TC CELL.

$$C \frac{dV}{dt} = -I_{Ca-T} - I_h - I_{KL} - I_{NL} - I_{GABA_A} - I_{GABA_B} \quad (2)$$

where  $I_h$  is the slow sag current, and the other currents are of the same types as in the RE cell, but with different gating kinetics, conductance strengths, and reversal potentials.

### Synaptic models

RE cells receive fast GABA<sub>A</sub>-mediated IPSPs from neighboring RE cells and fast AMPA-mediated excitatory postsynaptic potentials (EPSPs) from nearby TC cells (Bal et al. 1995b). TC cells receive both GABA<sub>A</sub> and GABA<sub>B</sub> IPSPs from nearby RE cells (Bal et al. 1995a). No recurrent excitation between TC cells is assumed (see Fig. 1A).

Our model neurons do not possess sodium spike-generating currents and exhibit only the slower low-threshold calcium spike (LTS) that underlies the bursts. Synaptic transmission occurs when the presynaptic cell depolarizes above a presumed threshold for action-potential firing; hence synaptic interactions can be viewed as calculated by averaging over the short time scales of a burst's action potentials. The gating variables  $s$  for AMPA and GABA<sub>A</sub> synapses, representing the fractions of open channels, are modeled according to (Wang and Rinzel 1992, 1993)

$$\frac{ds}{dt} = k_f S_\infty(V_{pre})(1 - s) - k_r s \quad (3)$$

where  $V_{pre}$  is the presynaptic potential,  $S_\infty(V) = \{1 + \exp[-(V - \theta_s)/\sigma_s]\}^{-1}$ ,  $\theta_s = -40$  mV being the presumed presynaptic voltage threshold for transmitter release and  $\sigma_s = 2$  mV. The parameters  $k_f$  and  $k_r$  for the AMPA and GABA<sub>A</sub> synapses are slightly different (see APPENDIX A). With this model, the peak synaptic current elicited by a brief presynaptic depolarization pulse is near saturation ( $s$  is close to 1), in accordance with experimental observations (Mody et al. 1994).

The slower GABA<sub>B</sub> inhibition is different. GABA<sub>B</sub>-mediated IPSPs are generally elicited at higher stimulus intensities than GABA<sub>A</sub>-mediated IPSPs; to date, there is no evidence that GABA<sub>B</sub> IPSPs occur either spontaneously or in response to a single spike in a presynaptic cell (Mody et al. 1994; Otis et al. 1993). These results indicate that the postsynaptic GABA<sub>B</sub>-mediated conductances can be activated only under specific conditions and that they operate far from saturation. Moreover, in the case of thalamic slice experiments, it was shown (Bal et al. 1995a,b; von Krosigk et al. 1993) that blocking GABA<sub>A</sub> receptors by bicuculline leads to significantly longer RE bursts, as well as higher spiking rate at the initial phase of the burst. Because our present model does not include sodium spikes, our mechanism for synaptic interactions is chosen to take the effect of this higher firing rate into account. Because the detailed mechanisms of GABA<sub>B</sub> activation are unknown, we model these experimental observations in a phenomenological way by assuming that the amplitude of the GABA<sub>B</sub>-driven conductance increases nonlinearly with the presynaptic burst duration. Synaptic gating is described by two differential equations

$$\frac{dx_B}{dt} = k_{fx} S_\infty(V_{pre})(1 - x_B) - k_{rx}[1 - S_\infty(V_{pre})]x_B \quad (4)$$

$$\frac{ds_B}{dt} = k_{fB} x_B^4 (1 - s_B) - k_{rB} s_B \quad (5)$$

where  $x_B$  corresponds to the activated G-protein level, and  $s_B$  is the fraction of open channels. This model synapse does not saturate easily and elicits significantly stronger responses to prolonged pre-synaptic bursts than to brief ones.

Axonal delays are neglected because they are expected to be no more than a few milliseconds, much smaller than the oscillation time period.

### Network architecture

The experiments of Bal et al. (1995a,b) and Kim et al. (1995) were performed on slices with typical dimensions  $5 \times 0.5 \times 0.5$  mm. Because the slice length was considerably larger than the width and depth, we consider a one-dimensional architecture. Our network model consists of  $N_{RE}$  RE neurons and  $N_{TC}$  TC neurons distributed equally along a straight line. The index  $i$  of an RE neuron,  $i = 1 \dots N_{RE}$ , represents its position along the line from left to right. The slice length,  $L$ , is constant and independent of  $N_{RE}$  and  $N_{TC}$ . The position of an RE (resp. TC) neuron with an index  $i$  is  $x_i = iL/N_{RE}$  (resp.  $iL/N_{TC}$ ). The synaptic coupling strength decays with the spatial distance between the pre- and postsynaptic cells. The connectivity diagram is shown in Fig. 1B.

The term "synaptic footprint shape" denotes the functional dependence of the synaptic connectivity on the distance between the pre- and postsynaptic cells. We assume, for simplicity, that this shape is symmetric. The coupling footprint length  $\lambda$  is the typical decay length of the synaptic footprint shape. It has subscripts denoting the type of the pre- and postsynaptic cells; in this model we have  $\lambda_{RR}$ ,  $\lambda_{RT}$ , and  $\lambda_{TR}$ . Two different footprint shapes are examined. For one, the synaptic coupling strength decays exponentially with the distance between the cells (as in Miles et al. 1988), to  $1/e$  of its peak value at an interneuronal distance  $\lambda$ . For our second footprint shape, synaptic coupling between a presynaptic cell at  $x_i$  and a postsynaptic cell at  $x_j$  is constant for  $|x_i - x_j| \leq \lambda$  and is

0 otherwise. The two coupling schemes are shown in Fig. 1C. Detailed anatomic and physiological data about the synaptic footprint shapes are presently not available. For simplicity, we assume throughout this paper that  $\lambda_{RR} = \lambda_{RT}$ .

Neurons near the slice edges receive synaptic inputs from their existing neighbors according to the same rule but do not get input from nonexistent “neurons” outside of the slice. Hence a neuron near the edge receives a smaller total amount of synaptic input. Except for that, all the RE cells and all the TC cells in the model are identical.

### Scaling of synaptic coupling

We investigate our model in a parameter regime defined by the two following conditions.

1. The synaptic footprint lengths are much smaller than the slice length:  $\lambda \ll L$  (for  $\lambda = \lambda_{RT}, \lambda_{RR}, \lambda_{TR}$ ). This ensures that edge effects are minimal and also leads to the consequence that a wavefront traverses the slice only after many cycles. Both  $L$  and the  $\lambda$ s remain fixed as  $N_{RE}$  or  $N_{TC}$  vary.

2. The number of cells within a footprint length is large:  $N \gg L/\lambda$  (for  $N = N_{RE}, N_{TC}$ ). A neuron receives synaptic inputs from many presynaptic neurons, and fluctuations in the total synaptic input to a cell are negligible.  $N$  is considered a discretization parameter, and each cell is representative of the neurons in a localized region of the slice.  $N$  should be large enough so that the computational results are not sensitive to the actual numbers of cells that are used.

The synaptic conductances between neurons are scaled according to these two conditions. The network dynamics should be independent of  $N_{RE}$  and  $N_{TC}$  (see Hansel and Sompolinsky 1996); as discretization parameters, they should be chosen large enough so that our model approximates well the neural tissue’s spatiotemporal behavior. In addition, we want to be able to distinguish between the effects of changing the total amount of synaptic input a neuron receives and the effects of coupling geometry. Consider for instance the TC-to-RE excitation. The maximal synaptic drive that an RE neuron  $i$  receives from a TC neuron  $j$  is given by  $g_{AMPA}w_{TR}(x_i, x_j)$  (Fig. 1B), where  $w_{TR}(x_i, x_j)$  is the footprint function and depends on  $(x_i - x_j)/\lambda_{TR}$  only. To ensure that the dynamics are insensitive to  $N_{TC}$ , we normalize  $w_{TR}$  such that

$$\sum_{j=-\infty}^{\infty} w_{TR}(x_i - x_j) = 1 \quad (6)$$

where the sum from 1 to  $N_{TC}$  was replaced by a sum from  $-\infty$  to  $\infty$ , ignoring edge effects and assuming that the neuron  $i$  is not located near the edges. A similar scaling applies to  $w_{RT}$  and  $w_{RR}$ . For simplicity, we take  $N_{RE} = N_{TC} = N$  and assume that all footprint lengths and distance quantities have been divided by the physical slice length, so that  $L = 1$ .

With this scaling, an increase in the presynaptic cell density would be incorporated in the model as an increase of the total synaptic coupling strength  $g$ , but not as an increase in  $N$ . Fluctuations in the total synaptic input may play a role when the number of presynaptic neurons is not large enough. In this case the dynamics may depend on the number of presynaptic neurons.

### Reference parameters and initial conditions

Not all the parameter values of our model can be determined from the existing experimental data. Moreover, as these values are varied, the model can exhibit a great variety of dynamical behaviors. As in our previous studies (Golomb et al. 1994a; Wang et al. 1995), we choose one set of reference parameter values that are consistent with many experimental results. These parameters are listed in APPENDIX A. Then we change systematically some parameter values in order to investigate their effects on the network dynamics.

Our goal is to understand the network dynamics associated with

the spindle wave propagation (Kim et al. 1995). Our model does not include waning of spindle episodes; the mechanisms responsible for the waning of spindle sequence oscillations are not yet known (Steriade et al. 1993; but see Destexhe et al. 1993 for a theoretical hypothesis). We model only the spindle onset and intraspindle behavior, as a propagating wavefront that recruits silent cells to oscillate. We initiate a wave by choosing appropriate initial conditions. At time  $t = 0$ , all the neurons are at their rest state, except for a few RE cells at the left end ( $i \leq 16$  in most simulations) that are depolarized to 0 mV. These neurons may recruit TC cells to burst and thereby initiate a wave of oscillating activity. Because the model does not include a “waning” mechanism, recruited neurons do not stop oscillating.

### Numerical and computational methods

The simulations reported in this paper were performed with the use of the fourth-order Runge-Kutta method with time step  $\Delta t = 0.5$  ms. We simulated networks with  $N$  between 128 and 512. Increasing  $N$  has little effect on the results as long as all the  $\lambda N$  values are large enough (say  $\geq 8$ ). The synaptic field that each neuron feels is given by a convolution of the synaptic coupling strength and the synaptic variable  $s$  from the presynaptic neurons (Eqs. A12, A13, A32, and A33). The convolutions were computed with the use of the fast Fourier transform (Press et al. 1989, section 12.4). A typical network simulation with  $N = 512$  and 10 s runs about 1 CPU h on an IBM-RISC-6000-375 workstation.

The wavefront velocity was computed as follows. When a neuron at position  $i$  had burst for the first time, and no neuron to its right had done so, the index  $i$  and the bursting time were recorded. The wavefront velocity was estimated by linear regression of all these space and time values. Separate calculations were performed for the RE and the TC populations for a consistency check.

The phase shift of neuronal bursting along the slice was calculated by linear regression through the position and the bursting time of neurons along one phase line. Only neurons far from the edges ( $0.2 \leq x_i \leq 0.8$ ) were included in order to minimize edge effects.

## RESULTS

### Single-cell dynamics

Both the RE and the TC cells are conditional oscillators (Golomb et al. 1994a). Depending on modulation of a potassium leak conductance or on constant injected current, each can be at rest or exhibit sustained oscillation. These two states may coexist and be realized by different initial conditions. The dynamical states exhibited by an isolated (RE or TC) cell are presented in Fig. 2A as  $g_{KL}$ , the potassium leak conductance of the cell, is varied. It is known that major neuromodulators such as acetylcholine, norepinephrine, and serotonin all influence and condition the occurrence of slow sleep rhythms in the thalamus, by modulating  $g_{KL}$  in TC and RE cells (McCormick 1992). In our model, an RE cell is at rest if  $g_{KL}$  is sufficiently small or sufficiently large, and it oscillates at intermediate  $g_{KL}$  values. Such low-frequency oscillations were recorded when the RE cell was depolarized (Lee and McCormick 1995; McCormick and Wang 1991). The TC cell behaves in a similar fashion and oscillates in an intermediate range of  $g_{KL}$  values.

Consistent with the experiments on the ferret slices (Bal et al. 1994a,b; von Krosigk et al. 1993) and on other preparations (Huguenard and Prince 1994; Warren et al. 1994), we choose the reference parameter set so our isolated RE and

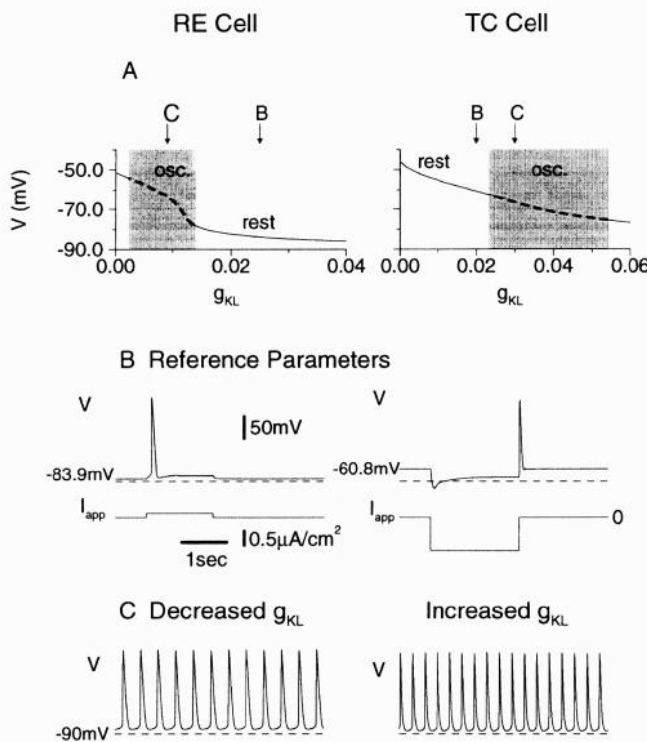


**FIG. 2.** Dynamics of single RE and TC cell models. *A*: the resting membrane potential vs.  $g_{KL}$  is represented by a solid line in the regimes where the rest state is stable and by a wide dashed line in the regime where it is unstable. Shaded areas represent the regime of endogenous oscillation. Bistability occurs in narrow regimes of overlap (on the right of the shaded area for the RE cell and on the left of the shaded area of the TC cell), where both the rest state and the periodic oscillations exist and are stable there. Arrows correspond to the parameters used for *B* and *C*. *B*: for the reference parameter set, the RE cell is at rest with a hyperpolarized membrane potential. Injection of a depolarizing current pulse of  $0.15\mu\text{A/cm}^2$  to the RE cell elicits a single burst. The TC cell is also resting, and it responds to release from a long-lasting hyperpolarizing current pulse (of  $-1.2\mu\text{A/cm}^2$ ) by a depolarizing sag followed by a postinhibitory rebound burst. *C*: membrane potential traces of RE and TC cells in the endogenously oscillatory regime.

TC cells are at rest. More specifically, the RE cell's  $V_{rest}$  is hyperpolarized, because its  $g_{KL}$  value is larger than  $g_{KL}$  in the oscillation regime (Fig. 2*B*). It responds to a brief depolarizing current pulse with a single burst. Steady moderate depolarizing current can drive it to oscillate. The TC cell's  $V_{rest}$  is more depolarized, and its  $g_{KL}$  value is smaller than  $g_{KL}$  in the oscillation regime. It requires hyperpolarization of sufficient duration so that it can respond, upon release or to a brief depolarizing current pulse, with a single rebound burst due to the T current (Deschénes et al. 1984; Jahnsen and Llinás 1984a,b; McCormick and Huguenard 1992; Pape et al. 1994; Wang et al. 1991). With a constant hyperpolarizing current of moderate intensity, it becomes oscillatory; but, with strong constant hyperpolarization, it is quiescent again. Membrane potential traces of cells, tuned into their rhythmically active regime, are presented in Fig. 2*C*.

#### Dynamics of $\text{GABA}_B$ synapses

In our  $\text{GABA}_B$  synaptic model, the slow  $\text{GABA}_B$  IPSPs depend nonlinearly on the duration of the presynaptic burst. Brief presynaptic RE bursts elicit weak  $\text{GABA}_B$  responses;

prolonged presynaptic RE bursts, as occur in the ferret slice experiments with  $\text{GABA}_A$  blockade (Bal et al. 1995b), result in much stronger  $\text{GABA}_B$  responses. This behavior is illustrated in Fig. 3, where an RE cell driven by a periodic external stimulus inhibits a TC cell via a  $\text{GABA}_B$  synapse only. No feedback excitation is included. In Fig. 3*A*, the intra-RE  $\text{GABA}_A$  coupling is represented by self-inhibition. Depolarizing current pulses are applied to the RE cell at 6.7 Hz, generating repetitive bursts with a duration of 48 ms. The  $\text{GABA}_B$  IPSPs are not strong enough, and the TC cell's response is subthreshold. In Fig. 3*B* the  $\text{GABA}_A$  self-inhibition is blocked, and the current pulses are injected at 3.3 Hz. The RE bursts are wider (96 ms) and produce much more powerful  $\text{GABA}_B$  IPSPs in the TC cell. This level of  $\text{GABA}_B$  inhibition hyperpolarizes the TC cell sufficiently to elicit PIR bursts.

#### Classification of bursting modes

The network dynamics behind the wavefront passage is similar to that of a network with all-to-all connectivity (Wang et al. 1995). The local population-averaged voltage

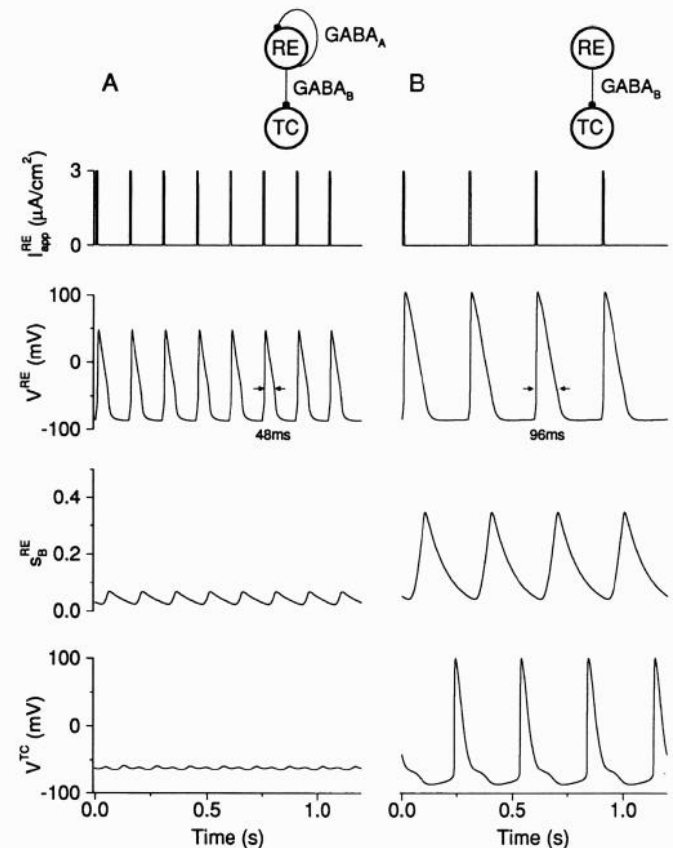


**FIG. 3.** Dynamics of  $\text{GABA}_B$  synapses. *A*: an RE cell is stimulated by periodic application of depolarizing current pulses at 6.7 Hz. It activates inhibitory postsynaptic potentials (IPSPs) in a TC cell with maximal  $\text{GABA}_B$  conductance of  $g_{\text{GABA}_B} = 0.06\text{ mS/cm}^2$ , as well as in itself with maximal  $\text{GABA}_A$  conductance of  $g_{\text{GABA}_A}^{RR} = 0.2\text{ mS/cm}^2$ . The  $\text{GABA}_B$  channel gating variable  $s_B^{RE}$  is too small to cause the TC cell to burst. *B*: the RE cell is driven at 3.3 Hz, and the intra-RE  $\text{GABA}_A$  inhibition is blocked. The RE cell bursts at 3.3 Hz, and the burst duration is doubled (96 ms as compared with 48 ms in *A*). The  $\text{GABA}_B$  gating variable  $s_B^{RE}$  is larger, and the TC cell is sufficiently hyperpolarized to produce rebound bursts.

(averaged over a local group of RE or TC neurons, within a length several times larger than  $\lambda_{RT} + \lambda_{TR}$ ) oscillates almost periodically with a frequency  $f$ . The local frequency  $f$  does not depend on position along the slice, except near the edges; it is the same for the RE and TC populations. RE cells usually fire bursts at almost every cycle, whereas TC cells do so only at every few cycles. We denote the bursting rate of the  $i$ th TC cell by  $\langle f_i \rangle_{TC}$  and the population-average bursting rate of all the TC cells by  $\langle f \rangle_{TC} = [\langle f_i \rangle_{TC}] (\cdot \cdot \cdot)$  denotes time averaging and  $[\cdot \cdot \cdot]$  denotes averaging over the population). Neurons near the edges are excluded. We define the bursting ratio of the TC population to be  $k_{TC} = f / \langle f \rangle_{TC}$ . Similarly,  $k_{RE} = f / \langle f \rangle_{RE}$  for the RE population. We define the bursting mode of the network to be  $k_{TC} : k_{RE}$ . For example, in a 1:1 mode both TC and RE cells fire bursts at every cycle, and in a 2:1 mode TC cells burst at half the frequency of RE cells. We use the terms “2:1” and “1:1” modes in a loose way, to refer to population averages, even if a few of the neurons burst with different rates.

#### *Population bursting and synaptic blockade*

The coupled RE-TC network with our particular choice of initial conditions exhibits a traveling front of spindle waves. A wavefront propagates at a constant velocity (modulo the lurching property) and corresponds to a moving transition between spatial regions of two different activity levels: neurons ahead of the wavefront are at rest, and the others, behind it, are oscillating. The oscillations persist because TC cells rebound from inhibition and reexcite the RE cells. Then the RE cells inhibit the TC cells again and deinactivate the T current, eliciting PIR bursts. In the “intact” slice model, a 2:1 bursting mode is observed with population frequency of 10.1 Hz. A rastergram of the cells’ firings is shown in Fig. 4A. Except for some irregularity near the front, neighboring RE cells tend to fire bursts simultaneously. We define bursting lines in the RE rastergram by connecting the bursting times of adjacent neurons. The lines are not exactly straight and parallel to the ordinate, revealing that the RE cells are not perfectly synchronized over long distances; following the bursting times of adjacent cells reveals a phase shift that varies (not necessarily monotonically) with the distance between cells. TC cells burst every second cycle. Cells tend to segregate into localized groups that fire simultaneously within groups; the typical group size increases linearly with the sum of footprint lengths  $\lambda_{TR} + \lambda_{RT}$  but depends on the details of the parameter set. The bursting behavior of the TC cells is also less regular near the front than far behind it. As seen for RE cells, there are phase shifts in the TC population, noticeable between widely separated groups.

Membrane potential traces of eight RE and eight TC neurons equally spaced along the slice are shown in Fig. 5A. A small minority of RE neurons skip every other oscillatory cycle. The first burst of RE cells lasts longer than the subsequent ones, because an RE cell at the wavefront receives less inhibition (i.e., only from cells behind the front) than afterward, and because in our model the T current of an RE cell at rest is considerably deinactivated. TC cells display prolonged hyperpolarization before their first burst. Two alternately bursting groups of TC cells can be identified; the phase shift between neurons within each group varies continuously with spatial position.

The burst firing rastergram with GABA<sub>B</sub> blockade is shown in Fig. 4B, and the membrane potential traces in Fig. 5B. The bursting pattern is similar to the previous case, because the GABA<sub>B</sub> IPSPs are small when the GABA<sub>A</sub> receptors are not blocked. In the absence of GABA<sub>B</sub> inhibition, the population frequency is increased slightly, to 10.7 Hz.

The effect of blocking GABA<sub>A</sub> receptors is prominent, as seen in Figs. 4C and 5C. The population frequency drops to 4.15 Hz, and the bursting pattern changes to 1:1; both RE and TC cells now fire bursts at every cycle. The irregularity of burst timing at the wavefront is reduced, although not completely, and the first RE burst is only slightly longer than the others. With the reference parameter set, the neurons are almost fully synchronized, and the phase shift is very small.

If both GABA<sub>A</sub> and GABA<sub>B</sub> are blocked, or if the AMPA excitation is blocked, the neurons are quiescent, and no wave propagation occurs (not shown). Thus our model is consistent with the six main experimental observations itemized in the INTRODUCTION.

The patterns shown in Fig. 4 are relatively regular, even in the 2:1 bursting mode. However, when certain model parameters were varied, more complex spatiotemporal patterns were seen in simulations, especially during the first several cycles following the wavefront passage. Irregularities such as skipped bursts may be seen as burst line terminations where a line of bursting events disappears at a certain point in a rastergram. Regions of differing spatiotemporal order can be separated by a curve of discontinuity in the bursting rastergram (reminiscent of dislocations in crystal growth patterns); neurons on either side of this curve, but nearby, burst regularly. We have also found cases in which the network starts to burst in the 1:1 mode and after several cycles switches to the 2:1 mode. These types of irregular behavior are illustrated in Fig. 6.

#### *Gradual suppression of GABA<sub>A</sub> inhibition*

Following the GABA<sub>A</sub> blocking experiment of Bal et al. (1995a), we investigate the dependence of the population frequency  $f$  (far behind the wavefront) on the GABA<sub>A</sub> coupling strength. As the GABA<sub>A</sub> conductance  $g_{GABA_A}$  is blocked gradually,  $f$  decreases slowly (Fig. 7). The main reason for this decrease is the reduction of intra-RE inhibition, which extends the RE burst duration and consequently extends the oscillation period. Although this result may appear counterintuitive, it is consistent with our previous observation that an enhancement of fast GABA<sub>A</sub> inhibition increases the population rhythmic frequency (Golomb et al. 1994a). At a particular  $g_{GABA_A}$  value,  $f$  drops suddenly and then continues decreasing slowly. The discontinuous frequency drop corresponds to a change of the bursting pattern from a 2:1 mode to a 1:1 mode. From a dynamical systems point of view, this is a transition between two qualitatively different states. The two states (2:1 and 1:1) coexist for a certain range of  $g_{GABA_A}$  values, where initial conditions would select the observed pattern. If we choose a specific initial condition, however, as we did while computing the diagrams in Fig. 7, there is a well-defined critical  $g_{GABA_A}$  value at which the transition occurs.

In Fig. 7 the population frequency versus  $g_{GABA_A}$  is plotted with two different values of the GABA<sub>B</sub> conductance

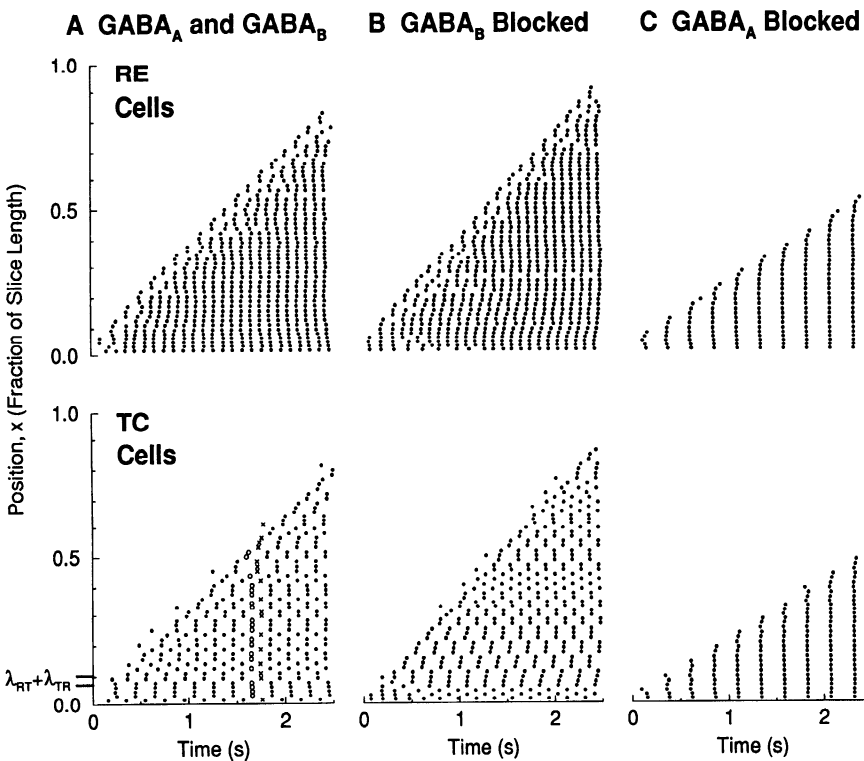


**FIG. 4.** Wavefront for transition from rest state to spindle oscillations: rastergram of RE cells (*top panels*) and TC cells (*bottom panels*). Simulations were performed with  $N = 512$  cells from each type and exponential footprint shape with  $\lambda_{RT} = \lambda_{TR} = \lambda = 0.0156$ . The length  $\lambda_{TR} + \lambda_{RT}$  is indicated on the bottom ordinate. Only the burst times from every 8th cell are shown. Arrows at the right indicate the positions of 8 RE cells and 8 TC cells along the slice whose voltage time courses are plotted in Fig. 5. Initially 16 RE cells at the left (small  $x$ ) are depolarized ( $V = 0$ ), and all the others are at rest. A wavefront propagates in all cases. *A*: in the presence of both GABA<sub>A</sub> and GABA<sub>B</sub> synapses, RE cells fire twice as often as TC cells (the 2:1 bursting mode), with a population rhythmic frequency  $f = 10.1$  Hz. The 2 groups of TC cells bursting alternately are denoted by open circles and crosses for 2 subsequent cycles. *B*: when GABA<sub>B</sub> synapses are blocked, the network behavior is similar, and the frequency  $f$  is increased by 6%. *C*: when GABA<sub>A</sub> synapses are blocked, the network oscillates at a lower frequency ( $f = 4.15$  Hz), RE and TC cells now fire in full synchrony and at the same frequency (the 1:1 bursting mode). When both the GABA<sub>A</sub> and GABA<sub>B</sub> inhibitions are blocked, or when the AMPA excitation is blocked, the network oscillation disappears, and the model slice is quiescent (not shown).

$g_{GABA_B}$ . Because the slow GABA<sub>B</sub> inhibition tends to favor the 1:1 state, with a  $g_{GABA_B}$  enhancement the transition from the 2:1 to 1:1 mode occurs at a larger  $g_{GABA_A}$  value. Furthermore, the population frequency is decreased with enhanced GABA<sub>B</sub> inhibition, because the TC cells are more hyperpolarized, and the T current deactivates more slowly before PIR bursts.

When the intra-RE GABA<sub>A</sub> inhibition is completely blocked, the network continues to oscillate (as shown in Wang et al. 1995). The frequency dependence on  $g_{GABA_A}$  is similar to the case with the intra-RE GABA<sub>A</sub> intact but with

a stronger GABA<sub>B</sub> inhibition (Fig. 7). This is because blocking intra-RE inhibition effectively enhances the GABA<sub>B</sub> inhibition in TC cells through a broadening of the RE burst. Above the transition, the population frequency is almost constant. Because the intra-RE inhibition is completely blocked, the RE burst duration does not change with GABA<sub>A</sub>.

We have also studied the effects of the excitatory AMPA maximal conductance  $g_{AMPA}$  on the bursting dynamics (not shown). For zero and very small  $g_{AMPA}$  values, the network is silent. Beyond a threshold  $g_{AMPA}$  value, 1:1 bursting oscil-

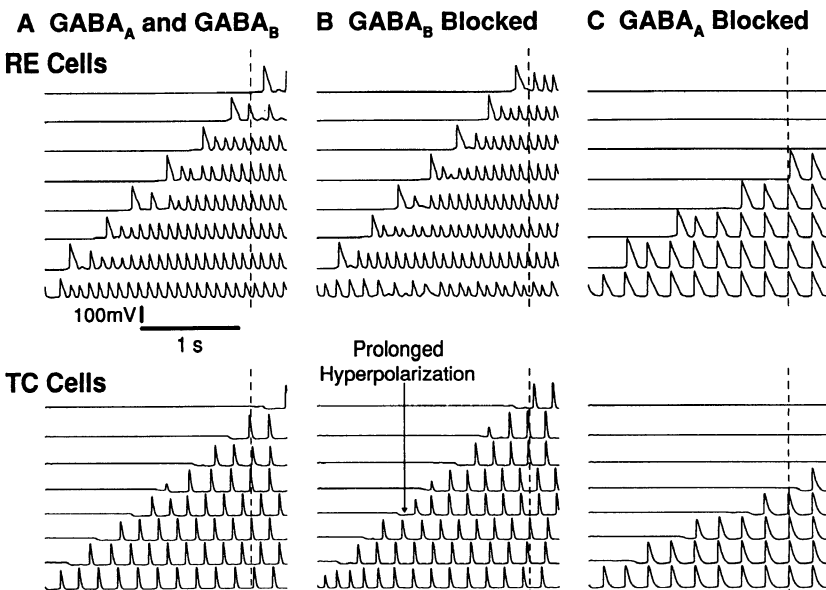


**FIG. 5.** Membrane potential time courses of 8 RE neurons and 8 TC neurons equally spaced along the slice between  $x = 0$  and  $x = 0.78$ , for the same simulation as shown in Fig. 4. Recording positions are indicated by the arrows in Fig. 4; time scale as in Fig. 4. Vertical dashed lines help to show how TC and RE cells fire in a 2:1 bursting mode when both GABA<sub>A</sub> and GABA<sub>B</sub> are intact (*A*) or when GABA<sub>B</sub> is blocked (*B*); and in a 1:1 bursting mode when GABA<sub>A</sub> is blocked (*C*). In the latter case (*C*), the phase shift between bursting neurons in this mode is close to 0 for our reference parameter set.

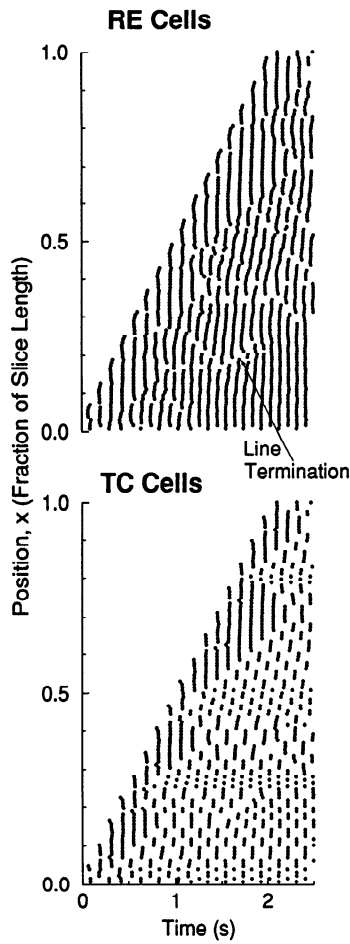


FIG. 6. Examples of irregularities in spatiotemporal spindling patterns: rastergram of RE cells (*top panel*) and TC cells (*bottom panel*). Simulations were performed with the same parameter set and initial conditions as in Fig. 4*B*, except for the RE-to-TC GABA<sub>A</sub> maximal conductance ( $g_{GABA_A} = 0.2 \text{ mS/cm}^2$  instead of  $0.1$ ) and the RE potassium leak conductance ( $g_{KL} = 0.035 \text{ mS/cm}^2$  instead of  $0.025$ ). Only the burst events of every 4th cell are shown. The network exhibits several types of irregular behavior, which are easier to follow in the RE than in the TC population. Just behind the wavefront the dynamical mode is 1:1, and it changes to 2:1 after several cycles. Spatiotemporal dislocations exist (e.g., near  $x = 0.18$  and  $x = 0.35$ ), where a bursting line breaks at a certain point and then is shifted to continue at a dislocated position. An example of a line termination is denoted by the arrow.

ations occur. In that regime, because the AMPA synapses are quite weak, synchronous inputs from most TC cells are needed to drive the RE cells to fire. Further increase of  $g_{AMPA}$  values transfers the network from the 1:1 to 2:1 bursting mode, where, because of the enhanced AMPA synapses, the firing of an RE cell no longer requires simultaneous activation of all its presynaptic TC cells, hence the 2:1 mode becomes possible. This transition would lead to a frequency jump, qualitatively like that in Fig. 7. To observe a robust 2:1 mode, the  $g_{AMPA}$  value should be several times higher than the threshold value at the onset of the 1:1 mode. For very strong AMPA excitation the bursting mode may switch to 3:1. Within each bursting mode, the oscillation population frequency is almost independent of the  $g_{AMPA}$  value.

#### Recruitment process

The wavefront propagation can be viewed as a recruitment process (Fig. 8). Here we follow the recruitment process in

a 1:1 state (with GABA<sub>A</sub> blocked), because in this mode the neuronal dynamics near the wavefronts is relatively regular and repeats itself as the wave propagates. In each step of the cycle (RE bursting or TC bursting), we define the wavefront location as the position of the rightmost RE or TC cell (with the largest  $x$ ) that bursts at this cycle. Suppose that at a certain time, RE cells behind the wavefront position have just fired a burst (Fig. 8*A*). These RE cells inhibit TC cells, including some within a distance (denoted by  $\rho_{RT}$ ) in front of the wavefront position. The TC cells remain hyperpolarized for a certain time interval (Fig. 8*B*), until the T current deinactivates sufficiently and these TC cells fire a rebound burst (Fig. 8*C*). At that moment the wavefront position moves forward by  $\rho_{RT}$  in the TC cell population, hence  $\rho_{RT}$  is the RE-to-TC recruitment length. During the rebound burst the TC cells in turn excite RE cells within a distance  $\rho_{TR}$  of the rightmost TC cell that has just burst;  $\rho_{TR}$  is the TC-to-RE recruitment length (Fig. 8*D*). The wavefront position is moved by an additional distance  $\rho_{TR}$ , and the cycle starts again. Hence the wavefront lurches forward instead of propagating continuously. The condition for net forward propagation is  $\rho_{RT} + \rho_{TR} > 0$ . In principle, one of the recruitment lengths could be negative. With the reference parameter set ( $g_{GABA_B} = 0.06 \text{ mS/cm}^2$  instead of  $0.12 \text{ mS/cm}^2$  in Fig. 8),  $\rho_{RT}$  is close to zero and much smaller than  $\rho_{TR}$ , and most of the recruitment is done via the AMPA excitation. With strong GABA<sub>A</sub> or GABA<sub>B</sub> conductances,  $\rho_{RT}$  may be larger than  $\rho_{TR}$  (see below).

The duration of an excitation-inhibition cycle at the front is often close to the oscillation period well behind the wave-

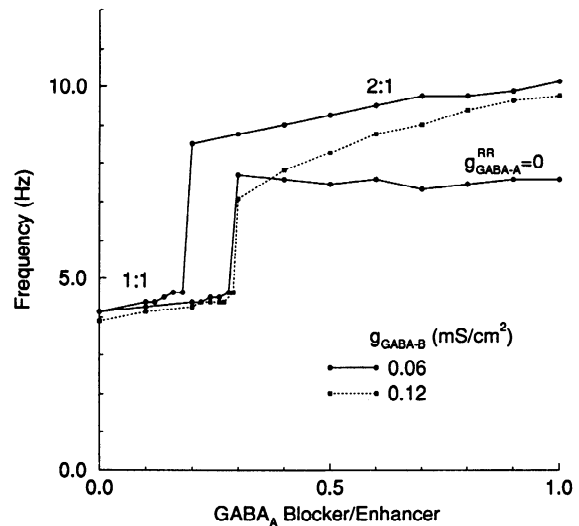


FIG. 7. Dependence of local population frequency on the maximal conductance of GABA<sub>A</sub> synapses. The population frequency is the same for the RE and TC populations. Almost all RE cells burst at this frequency, whereas TC cells burst at the same rate in the 1:1 mode and at  $\frac{1}{2}$  the rate in the 2:1 mode. The RE-to-TC and RE-to-RE GABA<sub>A</sub> conductances,  $g_{GABA_A}$  and  $g_{GABA_A}^{RR}$ , are equal to their reference values ( $0.1 \text{ mS/cm}^2$  and  $0.2 \text{ mS/cm}^2$ , respectively) multiplied by the blocker/enhancer level. Simulations were carried out with  $N = 512$  and exponential footprint shape with  $\lambda_{RT} = \lambda_{TR} = 0.0156$ . The local population frequency was calculated by averaging over 33 nearby RE cells. As GABA<sub>A</sub> is blocked, the oscillation frequency first decreases slowly and then drops discontinuously at a certain value, where a transition occurs from the 2:1 bursting mode to the 1:1 mode. If the GABA<sub>B</sub> coupling strength is strong ( $g_{GABA_B} = 0.12 \text{ mS/cm}^2$ ,  $\dots$ ), or if the intra-RE inhibition is completely blocked, the transition occurs at a larger  $g_{GABA_A}$  value.

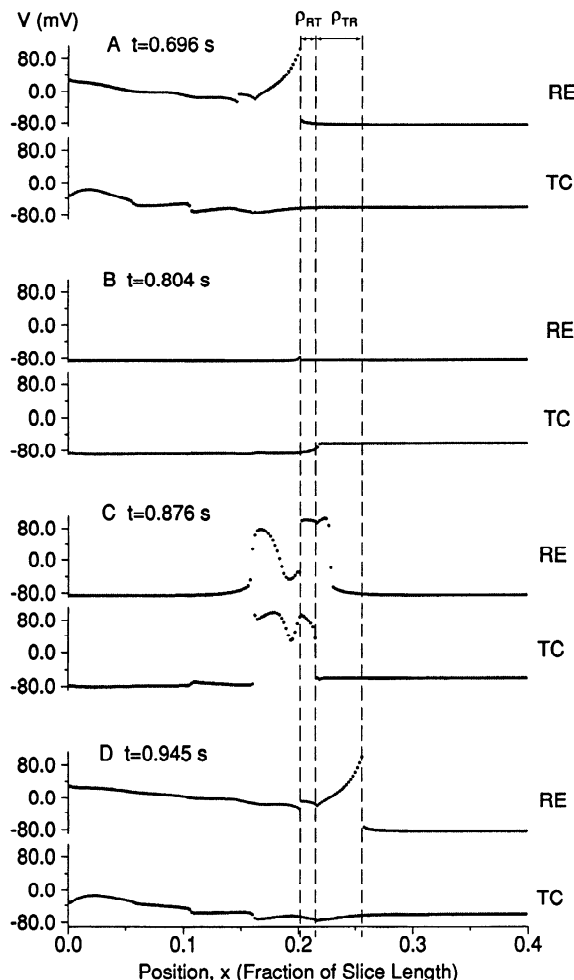


FIG. 8. Analysis of the lurching wave. Snapshots of the spatial profile along the slice of cells' membrane potentials, taken at 4 different times within a recruitment cycle (same parameters and initial conditions as in Fig. 4C, except for  $g_{\text{GABA}_B} = 0.12 \text{ mS/cm}^2$ ). Vertical dashed lines represent, from left to right, the wavefront position at subsequent steps of the recruitment cycle, corresponding to snapshots A, C, and D, respectively. A: RE cells fire a burst. B: RE cells are at rest, TC cells are hyperpolarized, including the cells within a distance  $\rho_{\text{RT}}$  ahead of the wavefront. C: TC cells within  $\rho_{\text{RT}}$  from the RE wavefront fire a rebound burst and excite the RE cells. RE cells start to burst. D: RE cells at a distance of  $\rho_{\text{TR}}$  ahead of the TC wavefront fire a burst, and the cycle starts again.

front, but in general the two do not have to be equal. In some cases, especially in a 2:1 bursting mode, the dynamics near the wavefront are more irregular, and distinct cycles may not be well defined.

We use the reference parameters (Fig. 4) to reproduce the wavefront propagation along a portion of the slice of 3 mm length covered by eight electrodes in the experiments of Kim et al. (1995). The wavefront takes  $\sim 30$  recruitment cycles in order to travel this distance. Relating this experimental recruitment length to the dimensionless one in our model, we conclude that the sum of the footprint lengths is  $\lambda_{\text{RT}} + \lambda_{\text{TR}} = 0.031$  (in terms of the fractions of the slice length). This sum thus corresponds to  $\sim 100 \mu\text{m}$  for a slice length of 3 mm. We will discuss the generality of this result later.

#### Wavefront velocity

**SIMPLE ANALYTIC ESTIMATE.** The wavefront velocity is defined as the spatial distance the wave has traveled divided

by the time needed for this propagation (measured over many recruitment cycles). This velocity does not depend on the position along the slice (far from the edges). Locally defined, wavefront velocity  $v_F$  equals the sum of the recruitment lengths  $\rho_{\text{RT}} + \rho_{\text{TR}}$  per recruitment period,  $T_{\text{rec}}$

$$v_F = \frac{\rho_{\text{RT}} + \rho_{\text{TR}}}{T_{\text{rec}}} \quad (7)$$

To obtain a simple estimate for  $v_F$  we approximate  $T_{\text{rec}}$  by the oscillation time period  $T$ , and in APPENDIX B we estimate the recruitment length (either  $\rho_{\text{RT}}$  or  $\rho_{\text{TR}}$ ), finding its approximate dependence on some parameters. We show that recruitment length scales linearly with the footprint length. For a step footprint shape, it (either from TC to RE or from RE to TC) is always smaller than the footprint length; it approaches the footprint length asymptotically with increasing synaptic coupling strengths. In the case of an exponential footprint shape, the recruitment length increases logarithmically with the synaptic coupling strengths, and it can be either smaller or larger than the footprint length. For all footprint shapes, in an intact network the RE-to-TC recruitment length depends mainly on the  $\text{GABA}_A$  maximal conductance  $g_{\text{GABA}_A}$ , because the  $\text{GABA}_B$  IPSPs are weak.

Several factors may cause discrepancies between our estimated  $v_F$  (from APPENDIX B and using  $T$  for  $T_{\text{rec}}$  in Eq. 7) and that obtained from simulations (as described in METHODS). First, the recruitment cycle time  $T_{\text{rec}}$  can differ from the oscillation period  $T$  away from the wavefront. Especially in the 2:1 state, the neuronal dynamics near the wavefront are irregular, making it difficult to define and measure the time duration of a recruitment cycle. Second, varying the synaptic conductances can alter qualitatively the global dynamics of the network, including the population frequency. For example, there may be a transition from a 2:1 state to a 1:1 state as a synaptic conductance is varied (sometimes a transition occurs after a few cycles behind the wavefront passage). The global dynamical change affects both  $T_{\text{rec}}$  and the  $\rho$  values, whereas this change is not accounted for by our velocity estimation (Eq. 7 and APPENDIX B). Third, if  $N\lambda_{\text{TR}}$  and  $N\lambda_{\text{RT}}$  are too small, finite size effects may play a role, and the velocity can deviate from the estimated value.

**SIMULATION RESULTS.** Numerical simulations have been performed in order to study the wavefront velocity's dependence on parameter values. Its dependence on the synaptic footprint length is presented in Fig. 9. The velocity is expressed as slice length per second. Calculations were carried out with  $\lambda_{\text{TR}} = \lambda_{\text{RT}} = \lambda$ , for both exponential and step footprint shapes, with or without the blockade of  $\text{GABA}_A$ . In all cases (and others we examined), the wavefront velocity  $v_F$  increases linearly with the footprint length, to very good accuracy. The simple estimate of  $v_F$  was calculated by assuming a step footprint shape,  $\text{GABA}_A$  synapses intact, a typical population frequency of 10 Hz, and equality between the recruitment lengths and the footprint lengths ( $\rho_{\text{RT}} = \lambda_{\text{RT}}$  and  $\rho_{\text{TR}} = \lambda_{\text{TR}}$ ). The actual wavefront velocity for the step footprint is smaller than this value for reasons discussed above.

The dependence of  $v_F$  on the synaptic conductance strengths is more complicated, as shown in Fig. 10. As expected from the simple estimate,  $v_F$  changes only slightly with the synaptic coupling strength in the case of a step footprint shape, except for small  $g_{\text{AMPA}}$  (Fig. 10C). The

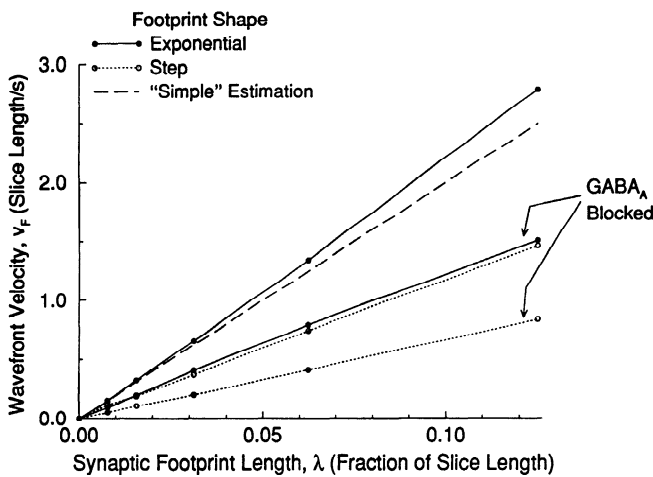


FIG. 9. Wavefront velocity  $v_F$  is plotted vs. the synaptic footprint length  $\lambda = \lambda_{RT} = \lambda_{TR}$ , for an exponential (—) or a step (· · ·) footprint shape. Simulations were done with or without GABA<sub>A</sub> blockade.  $N = 512$ . In all cases, the wavefront velocity increases linearly with the footprint length. Dashed line represents the simple analytic estimate (see text, *Simple analytic estimate*) of  $v_F$  for a step footprint shape, using an oscillation frequency of 10 Hz and an approximation of the recruitment lengths by the footprint lengths. The actual velocity for the step footprint is smaller than the simple estimate mostly because the recruitment lengths are smaller than the footprint lengths.

velocity  $v_F$  is smaller than the simple estimate. With an exponential footprint shape, the dependence of  $v_F$  on the coupling strength is more significant, and consistent with the estimated logarithmic relationship. Even though a sharp transition from a 2:1 mode to a 1:1 mode occurs far from the wavefront when the maximal GABA<sub>A</sub> conductance  $g_{GABA_A}$  is reduced beyond a critical value (Fig. 7), the wavefront velocity does not jump but decreases smoothly (Fig. 10A). The steep drop in  $v_F$  for small  $g_{AMPA}$  (Fig. 10C) is a result of the near-threshold behavior for the onset of network oscillations and is explained by our simple analytic estimate (see APPENDIX B).

Increasing the GABA<sub>B</sub> coupling strength results in two competing effects on  $v_F$ . On the one hand, it increases the recruitment length (especially for the exponential footprint shape); suggesting more cells being recruited per cycle. On the other hand, it hyperpolarizes the TC cells thereby increasing the oscillation period. As shown in Fig. 10B, the first effect dominates when GABA<sub>A</sub> is blocked (especially with exponential coupling); the wavefront velocity increases with the  $g_{GABA_B}$  value. When not blocked, GABA<sub>A</sub> determines the recruitment length, and the effect of GABA<sub>B</sub> is mainly to increase the period. Hence the wavefront velocity decreases with increasing  $g_{GABA_B}$  values.

We also assessed the sensitivity of the wavefront velocity  $v_F$  to two other aspects of the network model (Fig. 11). First, we consider the dependence of  $v_F$  on the potassium leak conductance  $g_{KL}$  in RE cells. With larger  $g_{KL}$  values, an RE cell is more hyperpolarized and needs to receive stronger EPSPs in order to fire a burst, hence the bursting threshold is effectively increased. Second, we consider the change of  $v_F$  when the connection footprint lengths differ in the two cell populations:  $\lambda_{RT} \neq \lambda_{TR}$ . With a step footprint shape,  $v_F$  shows a slight reduction with increasing  $g_{KL}$ , whether GABA<sub>A</sub> is blocked (Fig. 11B) or not (Fig. 11A). When either  $\lambda_{RT}$  or  $\lambda_{TR}$  is

reduced by a factor of 2,  $v_F$  is decreased by  $\sim \frac{1}{4}$ , as expected from our simple estimate. Figure 11, C and D, corresponds to the case of an exponential footprint shape. Consider first the case of GABA<sub>A</sub> synapses blocked (Fig. 11D). Here the recruitment is dominated by the TC-to-RE excitation, so decreasing  $\lambda_{TR}$  significantly decreases  $v_F$ . But, in the presence of GABA<sub>A</sub> inhibition (Fig. 11C), the RE-to-TC recruitment length exceeds the TC-to-RE recruitment length, and hence  $\lambda_{RT}$  has more effect than  $\lambda_{TR}$  on  $v_F$ .

### Phase shifts

In a 1:1 bursting mode, the phase shift is readily defined as the difference in bursting time between two neurons on the same bursting line. In a 2:1 mode without terminations or dislocations in bursting lines, the definition can be extended to RE cells that fire bursts at every cycle, whereas it is more difficult to do so for TC cells that fire bursts only at every few cycles. For this reason, we concentrate here on the 1:1 state with GABA<sub>A</sub> blocked and investigate the dependence of phase shift on parameters. When measuring phase shifts, we exclude neurons near the wavefront or the slice edges.

Although the phase shift of neurons for our reference parameter set is near zero (Fig. 4C), two cases with different parameters are shown in Fig. 12, A and B. In both cases, far from the edges and the wavefront, the phase shift grows linearly with the interneuronal distance. In A the phase shift is defined to be positive, as a neuron bursts before those to its right side. This case will be referred to as “delay,” because a neuron closer to the right edge bursts later. In B the phase shift is negative (“advance”), and a neuron fires a burst earlier than those to its left side.

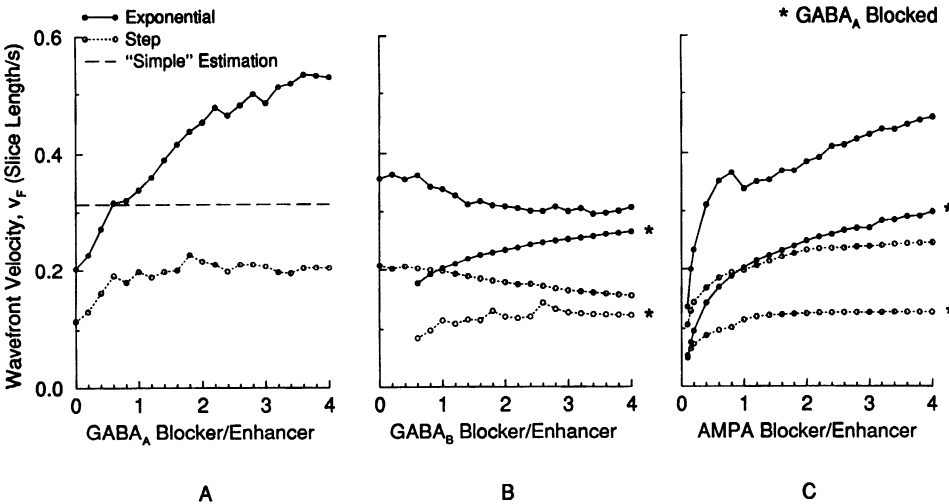
The phase shift is a transient phenomenon (APPENDIX C). We arbitrarily define the phase shift to be that of the phase line in which the wave has reached the right edge for the second time; this phase line is marked in Fig. 12, A and B. To use dimensionless units and make the comparison with experimental results easier, as explained in APPENDIX C, we define the normalized phase shift  $\mu$

$$\mu = \phi v_F \quad (8)$$

where  $\phi$  is the phase shift across the whole slice measured in seconds, and  $v_F$  is the wavefront velocity measured in 1/s (our slice length is normalized to 1).

The dependence of the normalized phase shift  $\mu$  on the RE potassium leak conductance  $g_{KL}$  is shown in Fig. 12C for several footprint lengths  $\lambda_{RT}$  and  $\lambda_{TR}$ . We see that the phase shift becomes more negative (advance) as  $g_{KL}$  of RE cells increases. Phase shifts develop because as the wavefront propagates, there is a difference in the bursting time between a neuron at the front (that is bursting for the 1st time) and a neuron behind the front (that has fired bursts previously). These results show that this difference becomes more negative as  $g_{KL}$  is increased and the RE cells are more hyperpolarized. Comparing the three curves in Fig. 12C, one sees that the phase shift becomes more negative (resp. positive) as  $\lambda_{TR}$  (resp.  $\lambda_{RT}$ ) is decreased.

When the bursting pattern is 2:1, the phase shift evolves in a more complicated way. The phase shift between neurons is no longer a linear function of their distance, and RE bursting lines can be curly (e.g., Fig. 4, A and B) or discontinuous (Fig. 6).



#### Heterogeneity and self-oscillating neurons

In our simulations we normally prescribe the initial conditions with most of the cells at rest except for a few depolarized RE cells at one end. This choice leads to traveling waves. With different initial conditions, various other patterns can be exhibited. For instance, if all the neurons start at rest, the network will stay quiescent. To observe spindle oscillations that emerge spontaneously from a totally quiescent network, without "stimulation at one edge," we introduced some heterogeneity in the intrinsic cellular properties. Here we assume heterogeneity in the potassium leak conductance  $g_{KL}$  of TC cells. The distribution function of  $g_{KL}$  is Gaussian with an average 0.02 mS/cm<sup>2</sup> (the original reference value) and a standard deviation 0.0025. TC neurons with strong enough  $g_{KL}$  are intrinsic oscillators (Fig. 2), and their resting state is unstable. Starting from near rest, they

FIG. 10. Dependence of the wavefront velocity  $v_F$  on the maximal synaptic conductances for GABA<sub>A</sub> (A), GABA<sub>B</sub> (B), or AMPA (C), measured here as the ratio with respect to their respective reference values (unity corresponds to the standard parameter set).  $N = 512$ ,  $\lambda_{RT} = \lambda_{TR} = 0.0156$ . Filled circles, exponential footprint shape; open circles, step footprint shape. Curves with the GABA<sub>A</sub> blockade are indicated by asterisks. Dashed line represents the simple analytic estimate (see Fig. 9). In general, the wavefront propagation is accelerated by increasing either the GABA<sub>A</sub> or AMPA coupling strength, more significantly so for the exponential than for the step footprint shape. The wavefront velocity decreases (resp. increases) with the GABA<sub>B</sub> coupling strength in the presence (resp. absence) of GABA<sub>A</sub> synapses.

eventually oscillate endogenously. If their excitation is sufficiently powerful to generate bursting in RE cells, or if there are enough oscillating TC cells that excite RE cells with the proper timing, a recruitment wave can be initiated at some point(s) in the slice, which will propagate in both directions. There can be several initiation points: for example, two in Fig. 13. When waves come from both directions, they coalesce and become synchronized after several cycles, as observed experimentally (Kim et al. 1995).

#### Do spindle oscillations require LTSs in RE cells?

In our model with the reference parameter set, both RE and TC cells exhibit LTSs and fire in a bursting mode. However, partially synchronous oscillations and wavefront propagation may still occur if the RE cells do not exhibit calcium LTSs. As a suggestive demonstration, we have sim-

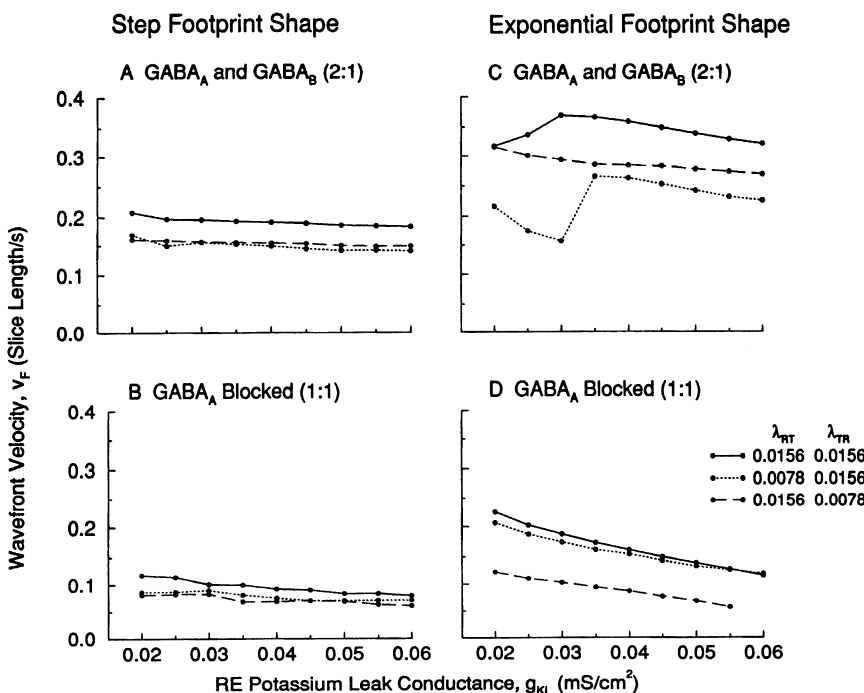


FIG. 11. Dependence of the wavefront velocity  $v_F$  on the RE potassium leak conductance  $g_{KL}$  for several values of footprint lengths  $\lambda_{RT}$  and  $\lambda_{TR}$ :  $\lambda_{RT} = 0.0156$ ,  $\lambda_{TR} = 0.0156$  (—),  $\lambda_{RT} = 0.0078$ ,  $\lambda_{TR} = 0.0156$  (· · ·), and  $\lambda_{RT} = 0.0156$ ,  $\lambda_{TR} = 0.0078$  (---).  $N = 512$ . The legend applies to all panels. In A and B the footprint shape is a step function, and in C and D it is exponential. In B and D the GABA<sub>A</sub> receptors are blocked. The bursting mode is 2:1 with GABA<sub>A</sub> intact and 1:1 with GABA<sub>A</sub> blockade. In C the jump in  $v_F$  at  $g_{KL} \approx 0.035$  mS/cm<sup>2</sup> is caused by a transition to the 1:1 bursting mode near the wavefront (the 2:1 mode is recovered far behind the wavefront).

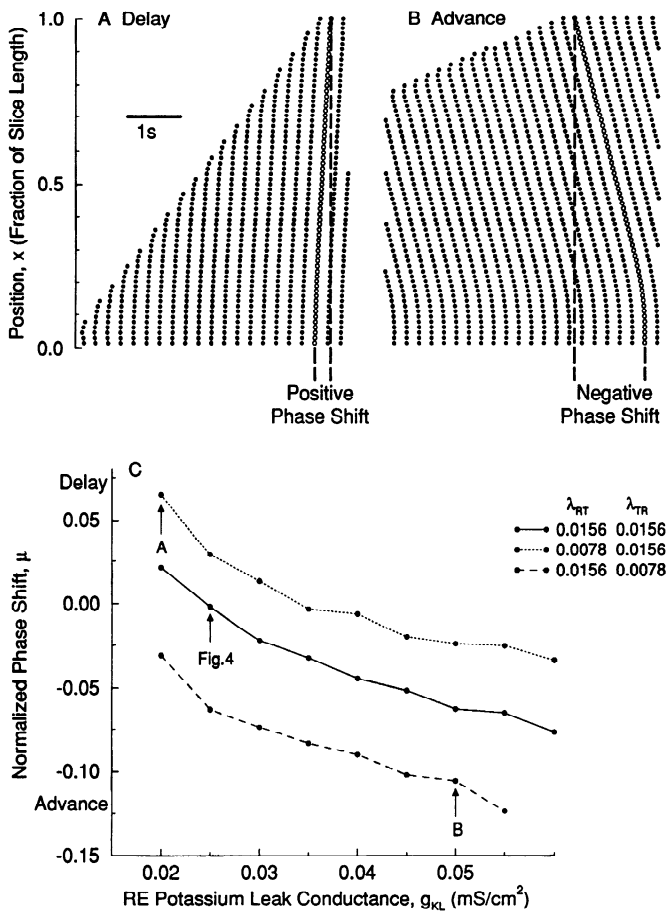


FIG. 12. Network can exhibit positive or negative phase shifts with  $\text{GABA}_A$  blockade. RE rastergrams are shown for every 8th cell. The footprint shape is exponential and  $N = 512$ . *A*: with RE  $g_{\text{KL}} = 0.02 \text{ mS/cm}^2$ ,  $\lambda_{\text{RT}} = 0.0078$ , and  $\lambda_{\text{TR}} = 0.0156$ , the phase shift is positive. A neuron fires bursts after those to its left. The phase shift was calculated with the use of the phase line indicated by the open circles, which is the phase line in which the wave's 2nd cycle has reached the right edge. *B*: with RE  $g_{\text{KL}} = 0.05 \text{ mS/cm}^2$ ,  $\lambda_{\text{RT}} = 0.0156$ , and  $\lambda_{\text{TR}} = 0.0078$ , the phase shift is negative. A neuron fires bursts before those to its left, as shown by the 2 vertical dashed lines that denote the edges of the chosen phase line. *C*: the dependence of the normalized phase shift  $\mu = \phi v_F$  (defined in APPENDIX C) on the RE  $g_{\text{KL}}$  value for 3 choices of  $\lambda_{\text{RT}}$  and  $\lambda_{\text{TR}}$  values:  $\lambda_{\text{RT}} = 0.0156$ ,  $\lambda_{\text{TR}} = 0.0156$  (—),  $\lambda_{\text{RT}} = 0.0078$ ,  $\lambda_{\text{TR}} = 0.0156$  (· · ·), and  $\lambda_{\text{RT}} = 0.0156$ ,  $\lambda_{\text{TR}} = 0.0078$  (— —). The wavefront velocity for these parameters is shown in Fig. 11*D*.

ulated this situation by blocking the calcium conductance  $g_{\text{Ca}}$  of the RE cells and increasing the AMPA conductance to  $g_{\text{AMPA}} = 0.5 \text{ mS/cm}^2$  (not shown). The network still displays a 2:1 bursting mode, although RE cells tend to skip more bursts. With  $\text{GABA}_A$  blocked, the network switches to a 1:1 bursting mode. The results are suggestive that minimal conditions for the oscillation are that RE cells depolarize adequately (to fire a train of spikes) in response to the excitatory drive that they receive from TC cells.

#### Oscillations in the isolated RE network

The reference parameter set was chosen for mimicking spindle rhythmicity in ferret thalamic slices. RE cells have a large  $g_{\text{KL}}$  value so that their resting potentials are hyperpolarized below the oscillatory regime (cf. Fig. 2*A*). As a

result, the isolated RE network, with mutual inhibition between its neurons, cannot oscillate without EPSPs from TC cells. However, if the  $g_{\text{KL}}$  value is smaller, a single RE cell can become oscillatory. Even if  $g_{\text{KL}}$  is below the oscillatory regime, a single RE cell is quiescent, but a network oscillation can result through mutual inhibition between RE cells (Destexhe et al. 1994b; Perkel and Mulloney 1972; Wang and Rinzel 1992, 1993). In both cases, the recurrent inhibition can induce some level of network synchrony (Steriade et al. 1987, 1990). To examine the isolated-RE oscillations with our one-dimensional connectivity architecture, we depolarized RE cells considerably by assuming that the nonspecific leak current has a conductance  $g_{\text{NL}} = 0.035 \text{ mS/cm}^2$  and reversal potential  $V_{\text{NL}} = -42 \text{ mV}$ . A single RE cell is resting at  $-56.9 \text{ mV}$ , but the RE network disconnected from the TC cell population can also oscillate (e.g., with  $\text{GABA}_A$  conductance of  $g_{\text{GABA}_A}^{RR} = 0.5 \text{ mS/cm}^2$ ). By choosing initial conditions where a few RE cells at the left edge of the slice are stimulated, a wavefront is initiated and propagates from left to right, as shown in Fig. 14. After the wavefront has passed, the population oscillates with a frequency of 16.6 Hz, similar to the higher frequencies sometimes ob-

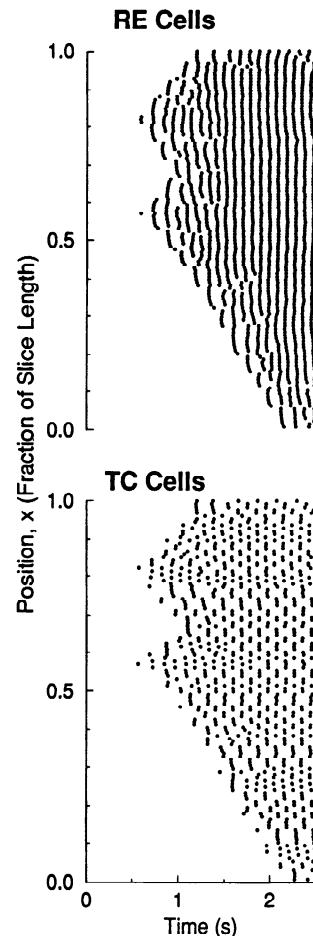


FIG. 13. TC cells that are intrinsic oscillators can initiate a wave. The TC potassium leak conductance  $g_{\text{KL}}$  is chosen randomly from a Gaussian distribution with an average  $0.02 \text{ mS/cm}^2$  and a standard deviation  $0.0025 \text{ mS/cm}^2$ . A network with  $N = 128$ , exponential footprint shape and  $\lambda_{\text{RT}} = \lambda_{\text{TR}} = 0.0156$  starts when all the cells are at rest. Bursts of all the cells are shown in the rastergram. Two cells that are intrinsic oscillators initiate waves that propagate in both directions.

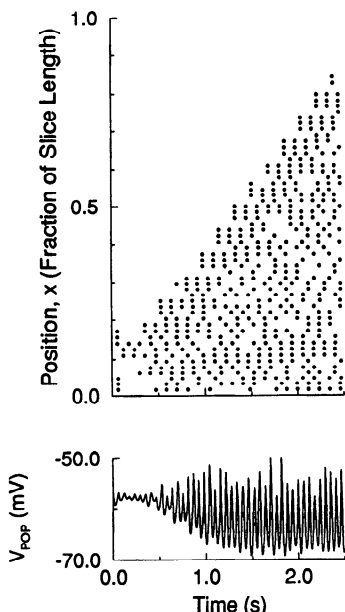


FIG. 14. Wave propagation in an isolated RE network. Here RE cells are less hyperpolarized as compared with our reference parameter set. Every 2nd cell from the RE population is shown in the rastergram (*top panel*). The local population voltage, averaged over neurons located at  $0.25 \leq x \leq 0.5$ , is presented in the *bottom panel*. Simulations were carried out with  $N = 128$ , an exponential footprint shape with  $\lambda_{\text{RR}} = 0.0625$ , maximal GABA<sub>A</sub> conductance  $g_{\text{GABA}_A}^{\text{RR}} = 0.5 \text{ mS/cm}^2$ , and potassium leak conductance  $g_{\text{KL}} = 0.025 \text{ mS/cm}^2$ . The nonspecific leak current has a conductance  $g_{\text{NL}} = 0.035 \text{ mS/cm}^2$  and a reversal potential  $V_{\text{NL}} = -42 \text{ mV}$ .

served experimentally in the *in vivo* segregated reticularis (Steriade et al. 1987). In the example of Fig. 14, each RE cell fires bursts every second or third, or more, cycles. Note that a subset of neurons that fire bursts at the same cycle are highly synchronized and the phase shift is small. Because with different parameters a network with all-to-all coupling may exhibit many kinds of partially synchronized patterns, we can expect to get various patterns here as well. In particular, we found patterns in which some RE neurons oscillate, whereas others are quiescent (not shown).

## DISCUSSION

We have developed a one-dimensional model of thalamic slices that exhibits wavefront propagation. Ahead of the wavefront the neurons are quiescent; behind it they oscillate with a high degree of synchrony. Even a model as idealized as ours can in general exhibit many spatiotemporal patterns. However, this model, with the chosen reference parameter set, can duplicate at least the six main experimental observations about the network dynamics, obtained by McCormick and colleagues (Bal et al. 1995a,b; Kim et al. 1995; von Krosigk et al. 1993) and listed in the INTRODUCTION. In addition, it is consistent with the experimental data from voltage-clamp and current-clamp recordings on the intrinsic ionic currents in TC and RE cells as well as on the properties of synaptic transmission in the thalamus. The model's ability to reproduce all these results, while fulfilling and illuminating the known biological constraints (especially with respect to the synaptic kinetics), represents a main result of this work.

Our model demonstrates the lurching characteristics of the recruitment process. Aspects of the wavefront propagation are affected by both intrinsic and network properties. The wavefront velocity is limited by the postinhibitory rebound properties of TC cells (intrinsic) and by the spatially localized synaptic footprints (network). The wave speed increases linearly with the footprint lengths but only gradually with the synaptic coupling strengths, and it decreases gradually with enhanced hyperpolarization of the RE cell population. We showed that these dependencies are themselves functions of the synaptic footprint shapes and are more sensitive when the footprint decays more gradually with the distance between the pre- and postsynaptic cells. The model shows that when GABA<sub>A</sub> is blocked, the phase shift between a pair of cells increases linearly with the interneuronal distance. However, it does not predict the magnitude of the phase shift itself. Depending on parameter tuning, it can be positive, negative, or near zero. We suggest that, in addition to a propagating wavefront, the network can exhibit many other spatiotemporal patterns. For example, small localized concentrations of intrinsic oscillators can create many wave initiation points. The system behavior depends quantitatively, but generally not qualitatively, on the synaptic footprint shape.

## Single-cell properties and network behavior

The model's TC cells fire bursts in subharmonics with the population rhythm, at every other cycle (the 2:1 bursting mode) or less frequently. As was shown previously (Kopell and LeMasson 1994; Wang 1994; Wang et al. 1995), the presence of the hyperpolarization-activated cation current ( $I_h$ ) is crucial in order to enable the TC cell to burst every second time in a robust way. A burst deactivates  $I_h$ , and then at least two population cycles (at 10 Hz) are required for the inward  $I_h$  to build up, enabling the cell to burst again. A reduction of the maximal  $I_h$  conductance  $g_h$  leads to a hyperpolarization of TC cells. A moderate decrease of  $g_h$  can be compensated by an increased activation of the  $I_h$  channels at the hyperpolarized voltages, so that the  $I_h$  amplitude is little changed, and the 2:1 bursting mode may still be robust. With complete  $g_h$  blockade, TC cells are further hyperpolarized, and as a consequence the  $I_h$  current may become slow enough so that the 2:1 bursting mode is still possible. However, without the  $I_h$ , this 2:1 mode was seen in our model simulations only in a very restricted parameter regime.

Our single-cell models have only one compartment, for the sake of simplicity. This assumption seems reasonable for the TC cells that appear to be electrically compact (Bloomfield et al. 1987; McCormick and Huguenard 1992). The cable properties of RE cells are less well characterized; and although evidence suggests the presence of a significant amount of T conductance on the dendrites (Contreras et al. 1993), the spatial distribution of active conductances on RE cells has not been quantified. The one-compartment idealization has an effect on the resting state of our RE and TC model cells. For the reference parameter set, the TC cell's  $V_{\text{rest}} = -60.8 \text{ mV}$ , differs from the experimental measurement of about  $-70 \text{ mV}$  (Bal et al. 1995a), and the RE cell's  $V_{\text{rest}} = -83.9 \text{ mV}$ , is more negative than that reported  $-67 \text{ mV}$  by

Bal et al. (1995b). Bal et al. (1995a,b) suggested that a gradual hyperpolarization of a RE cell would increasingly raise the effective bursting threshold in these cells, until the EPSPs from TC cells would be no longer powerful enough to reach that threshold, so that the RE cell could not fire bursts anymore. We tested this scenario in our model by increasing the potassium leak conductance  $g_{KL}$  in RE cells. Significant enhancement of  $g_{KL}$  was seen to reduce the wave-front velocity but did not abolish burst firing of RE cells nor the spindles in the RE-TC network. Improvements of the present thalamic model, such as a more elaborate compartmental modeling of RE cells and the inclusion of sodium spikes, may resolve these disagreements.

To account for the six experimental results from ferret slice, the model RE neurons must operate in the bursting mode where the calcium T conductance is prominent. On the other hand, we found in simulations that network oscillations can still persist even if this T conductance is blocked in RE cells.

#### *Saturation and nonlinearity in synaptic response*

The study of synaptic transmission is generally concerned with unitary postsynaptic potential or current elicited by a single presynaptic action potential, and much less is known about how a postsynaptic receptor temporally integrates the stimulus by a train of presynaptic action potentials. Traditionally, theoreticians have used the form of the  $\alpha$ -function and its extensions (Destexhe et al. 1994c; Koch and Segev 1989; Rall 1967), and the postsynaptic conductance response to a barrage of presynaptic action potentials is modeled as a simple sum of individual responses. In reality, deviations from linearity may occur. Postsynaptic conductances can saturate, so that the response to the consecutive action potentials is less than expected from linear addition. There are experimental indications for saturation of AMPA and GABA<sub>A</sub> synapses (Mody et al. 1994). On the other hand, GABA<sub>B</sub> synapses seem to display a significant response only to sufficiently strong stimuli, but not to weak stimuli (Mody et al. 1994), indicating that the GABA<sub>B</sub> response to a barrage of action potentials is larger than expected by the linear approximation.

In the present model, spike-generating currents are not included, and the nonlinear integration of synaptic responses is carried out in terms of burst duration, which is assumed to increase with the number of repetitive spikes in a burst. The firing rate within a burst is usually not constant. For example, an RE cell's burst consists of more spikes with the GABA<sub>A</sub> blockade than in the intact situation, not only because the burst is much prolonged, but also the firing rate becomes very high at the beginning of the burst (Bal et al. 1995b).

Given these limitations, as a first step toward biophysical modeling of GABA<sub>B</sub> synaptic transmission, we formulated a phenomenological model that is both consistent with the above synaptic data and enables us to reproduce the ferret thalamic slice experiments. As in our previous models, the AMPA and GABA<sub>A</sub> synaptic models operate near saturation. However, the GABA<sub>B</sub> synapses do not reach saturation, and their response increases nonlinearly with the presynaptic burst duration. We hypothesize that this burst-duration-de-

pendent response is a result of both the increased number of spikes on a wider burst and the nonlinear properties of the GABA<sub>B</sub> receptors.

The GABA<sub>B</sub> model with its burst-duration dependence helps us to explain two of the ferret slice characteristics. First, GABA<sub>B</sub> synapses have almost no effect on spindle oscillations in the intact slice, yet they can support the slow synchronized oscillations when GABA<sub>A</sub> is blocked. To understand this, suppose the GABA<sub>B</sub> synapses were effective in the intact slice. Then they would hyperpolarize TC cells (because of their negative reversal potential and slow decay), thereby slowing the T-current kinetics and hence slowing the rebound process in these cells. A GABA<sub>B</sub> blockade should then result in abolishing this effect and consequently in an increase of the TC population oscillation frequency. Because only little change is seen experimentally, GABA<sub>B</sub> IPSPs ought to be weak when GABA<sub>A</sub> IPSPs are not blocked. This is consistent with our model, because the RE burst duration with GABA<sub>A</sub> intact is relatively small, and hence the GABA<sub>B</sub> synaptic response fluctuates at low levels (Fig. 2). Note that the RE burst is narrower in the intact case for two reasons: 1) the intra-RE GABA<sub>A</sub> inhibition cuts short the RE bursts, and 2) at the relatively high ( $\approx 10$  Hz) frequency, the T current is not fully deinactivated and the bursts are weaker and shorter in time.

Second, the burst-duration dependence of the GABA<sub>B</sub> synapses is also important for robustly generating the slow synchronous 1:1 oscillation when GABA<sub>A</sub> is blocked in the model. In our previous work (Wang et al. 1995), although we were able (by choosing initial conditions in an appropriate range) to reproduce this 1:1 bursting mode in the absence of GABA<sub>A</sub> inhibition, it often coexisted with another, asynchronous oscillatory state. We believe that the asynchronous state was present, because the GABA<sub>B</sub> model synapse in Wang et al. (1995) was not endowed with the nonlinear kinetic property postulated in the present GABA<sub>B</sub> model. That previous GABA<sub>B</sub> synapse model could saturate from the much prolonged bursts of the presynaptic RE cells in the absence of GABA<sub>A</sub> inhibition. In that case the RE-to-TC GABA<sub>B</sub> IPSPs provided a quasi-constant hyperpolarization and would not phasically synchronize the TC cells. Indeed, with the present GABA<sub>B</sub> model, the asynchronous state has not been observed in simulations, both for the present spatially dependent connectivity and for the random connectivity as in Wang et al. (1995).

These results illustrate how details of synaptic kinetics and integration mechanisms may affect network dynamics qualitatively. Destexhe and Sejnowski (1995) suggest that kinetic properties of the G-protein transduction mechanism underlie the strong GABA<sub>B</sub> response to prolonged bursts. In their model, the variable representing the G-protein concentration was raised to the fourth power due to G-protein cooperativity. In our phenomenological model, the variable  $x_B$  (Eq. 4) is interpreted as the activated G-protein concentration, whereas the variable  $s_B$  corresponds to the activation of GABA<sub>B</sub> channels with kinetics that depend on the fourth power of  $x_B$ . In our case the gating kinetics of the GABA<sub>B</sub> channels is relatively slow, in contrast to that in the model of Destexhe and Sejnowski, where channel opening and closing depend instantaneously on G-protein concentration. More experimental and theoretical work is needed to test our hy-

pothesis and understand the GABA<sub>B</sub> activation and synaptic integration processing at the biophysical level.

The bursting mode depends also on the strength of the AMPA synapses. With AMPA excitation partially blocked (and GABA<sub>A</sub> not blocked), the system tends to burst in a 1:1 mode.

#### *Network dynamics in one-dimensional models and sparseness effects*

In our model, synaptic weights are normalized so that the total synaptic drive (of a given type) is the same to cells at different positions but away from the edges. Furthermore, the maximal synaptic conductances ( $g$  values) implicitly include the effect of local cell densities, because they are the product of presynaptic cell density and single afferent conductance. This prescription is reasonable biologically only if in the thalamic circuit fluctuations in synaptic inputs among cells are small, i.e., when the number of cells that make sufficiently strong synaptic contacts with a single postsynaptic cell is large enough. In the real slice the synaptic connectivity may be anatomically sparse, and a cell may receive functionally strong synapses only from a few other cells. These fluctuations affect the dynamics and reduce the synchrony among cells (Barkai et al. 1990; Wang et al. 1995).

The intact slice model bursts in a 2:1 mode after the wavefront passes. In this state, we can visually identify two clusters of TC cells that burst together globally, even though we cannot define them precisely because of phase shifts and the spatial gradient in burst timing. However, this state can be regarded as an extension of the cluster states found in globally connected network models (e.g., Golomb and Rinzel 1993, 1994; Golomb et al. 1994a,b, 1995; Wang et al. 1995). Both are examples of spontaneous symmetry breaking; in the present case of a long slice, translation symmetry is broken (Anderson and Stein 1984). The segregation of TC cells into two approximate clusters creates spatially contiguous groupings where all the neurons within each group burst almost simultaneously. The spatial group size varies, but the typical length increases with the footprint length. This grouping is presumably a result of the homogeneity of cellular and coupling properties in our model. The introduction of randomness and sparseness to the spatially dependent connectivity might eliminate these contiguous groups (Wang et al. 1995).

Bursting patterns where TC cells fire at a lower frequency ratio than the 2:1 mode (such as 3:1, 4:1) can be obtained if the TC cells are more hyperpolarized or if the h conductance is decreased. However, these changes usually make the TC cell an intrinsic oscillator. Sparseness is expected to cause both RE and TC cells to skip bursts, as found in a model with spatially independent but sparse connectivity (Wang et al. 1995).

Another result that is affected by sparseness is the sharp transition between the 2:1 and 1:1 modes, accompanied by a population frequency drop, as the GABA<sub>A</sub> receptors are gradually blocked (Fig. 7). By contrast, in the experiments of Bal et al. (1995a), the change of the population rhythmic frequency is continuous. Sparseness and heterogeneity would smooth the curve and smear the transition.

#### *Recruitment and wavefront propagation*

In our simulations, the process of recruiting cells into the oscillatory mode displays lurching and discontinuous characteristics. At each step, RE cells recruit a new group of downstream TC cells. These cells are hyperpolarized for a large portion of the cycle before they fire a rebound burst and then recruit the next new group of RE cells. The lurching wave differs from other processes of recruitment, such as action-potential propagation along an unmyelinated axon as more inward current sources are recruited continuously (Hodgkin and Huxley 1952), or continuous wave propagation by synaptic excitation (Chervin et al. 1988; Ermentrout and McLeod 1993; Idiart and Abbott 1993; Miles et al. 1988; Traub et al. 1993).

The wavefront propagation velocity  $v_F$  in thalamic slice,  $\sim 1$  mm/s, is slow in comparison with wavefront velocities of excitation in other slice preparation, such as 60 mm/s in cortical slices and 140 mm/s in hippocampal slices (Chervin et al. 1988; Miles et al. 1988; Traub et al. 1993). The synaptic footprint shapes are assumed here to be spatially symmetric. The wavefront's speed depends on the propagation direction for asymmetric footprint shapes.

Kim et al. (1995) reported that a spindle wave needed  $\approx 30$  cycles in order to pass along a slice distance of  $\approx 3$  mm. This implies, in the context of our model, that the sum of the recruitment lengths  $\rho_{RT} + \rho_{TR}$  is  $\approx 100$   $\mu\text{m}$ . Our model relates the recruitment lengths, measured from physiology, to the footprint lengths, that can be measured anatomically. It shows that the sum of the footprint lengths cannot be significantly larger, because the recruitment length is much smaller than the footprint length only when the corresponding synaptic coupling strength is just above threshold for the onset of network spindle oscillations. However, in this just-suprathreshold parameter regime the system behavior is not robust and does not display features of the six main experimental observations (see INTRODUCTION). Our simulations show that for maintaining a stable 2:1 state, the maximal AMPA-conductance  $g_{AMPA}$  should be several times stronger than its threshold value for oscillations. The maximal GABA<sub>A</sub> conductance  $g_{GABA_A}$  should also be much stronger than its threshold value; otherwise the effects of blocking GABA<sub>B</sub> would be clearly seen in experiments. Therefore the experimental results of Kim et al. together with our model's results suggest that the reciprocal synaptic projections between RE and TC cells should both be spatially localized, on the order of 100  $\mu\text{m}$ .

What are the anatomic data for the footprint lengths? In cat LGN, the spatial extents of the dendritic and axonal trees of RE and TC cells were studied by intracellular staining and by electron microscopy, but their quantitative and statistical characterizations remain far from complete. Roughly speaking, the dendritic arborizations of RE cells can extend for several hundred micrometers; whereas their axonal projections in the TC vary from being very restricted to widespread (up to 200–300  $\mu\text{m}$ ) (Cucchiaro et al. 1991; Uhrlrich et al. 1991). The dendritic trees of TC cells extend for 100  $\mu\text{m}$  (the X-type LGN cell) to 200–400  $\mu\text{m}$  (the Y-type LGN cell) (Friedlander et al. 1981; Sherman and Koch 1990), and the synaptic contacts from RE cells are located mostly in the distal dendrites (Cucchiaro et al.

1991). The TC collaterals in the RE can be short or extensive (up to a few hundred  $\mu\text{m}$ ) (Friedlander et al. 1981; see also Harris 1987 on the rat somatosensory thalamus); and the contacts seem to be made predominantly near the RE cell body (Ide 1982).

These anatomic data from cats indicate that if the RE-TC coupling were random, the sum of the reciprocal synaptic footprint lengths would be  $>100 \mu\text{m}$ . Admittedly, the morphology of the ferret LGN and PGN cells may be different from those in cat. On the other hand, the spindle wave propagation velocity as seen from *in vivo* simultaneous recording in cats under pentobarbitone anesthetics seems as slow as in the ferret slices (Andersen et al. 1966). To reconcile the predicted short footprint lengths with the morphological data, more information is needed about the reciprocal RE-TC projections. For instance, the dendritic or axonal arborization of a thalamic cell is often anisotropic (Pinault et al. 1995), and we do not know the extents of the axonal and dendritic trees in the direction of the wave propagation. Moreover, the probability of synaptic contacts or the synaptic strengths likely vary along the dendritic and axonal trees; these distributions remain to be assessed.

#### Phase shifts

In the 1:1 bursting mode, the relative phase shift grows linearly with the distance between a pair of neurons. The model's phase gradients depend sensitively on parameters; positive, negative, or near zero phase shifts are found. On the other hand, the model may predict the trends when parameters are changed. Being dependent on the network's transient behavior near the wavefront, the phase shift is expected to be affected by the waxing and waning of the spindle oscillations. Hence quantitative differences between the model's results regarding phase shifts and future experimental observations may be found.

#### Significance of the intra-RE connections

The intra-RE synaptic interconnections via fast GABA<sub>A</sub> synapses play a dual role with regard to the thalamic oscillations. On the one hand, under certain conditions they enable the RE network alone to generate population oscillations in the spindle frequency range, as shown experimentally (Steriade et al. 1987), and in computational models with global or spatially dependent connectivity (Destexhe et al. 1994a,b; Golomb and Rinzel 1993, 1994; Golomb et al. 1994a, 1995; Wang and Rinzel 1992, 1993). Here we show that this oscillation can also occur in a one-dimensional architecture, when RE cells are less hyperpolarized; the RE network model displays wavefront propagation for appropriate initial conditions. This is similar to *in vivo* experimental results (Steriade et al. 1987) showing oscillating spots in the rostral pole, whereas adjacent spots were quiescent. In this preparation, such reduction of the hyperpolarization of RE cells may be due to the depolarizing effect of norepinephrine and serotonin modulatory systems.

On the other hand, even when the intra-RE coupling is not essential for rhythmogenesis, we see that it strongly affects the RE-TC network behavior especially by reducing the burst duration of RE cells and hence the amplitude of

the RE-generated slow GABA<sub>B</sub> IPSPs in TC cells, as also seen experimentally (Huguenard and Prince 1994). In some parameter regimes, blocking the intra-RE coupling can transform the bursting mode from 2:1 into 1:1.

#### Experimentally testable results

To summarize, we list here some of the model's main results that ought to be experimentally testable in ferret thalamic slices. 1) The GABA<sub>B</sub> receptors of the RE-to-TC projections operate far from saturation and respond much more strongly to a prolonged burst than to a brief one. Here, one might employ paired recordings with the assist of infrared video microscopy as in recent work of Sakmann and colleagues (Markram and Sakmann 1995). 2) The wavefront propagates in a lurching manner, especially in the 1:1 mode, where in each cycle a distinct group of RE and TC cells are recruited. Imaging, either by calcium or voltage-sensitive dyes, may adequately resolve the spatiotemporal profiles to detect this feature. 3) Oscillations persist if the intra-RE inhibition is blocked. As in Huguenard and Prince (1994), local application of bicuculline to the RE region should be attempted, possibly with the assistance of mild pressure by a sharp edge along the RE-TC border. 4) The RE-to-TC and the TC-to-RE footprint lengths are spatially restricted, with their sum around  $100 \mu\text{m}$ . Here also, paired recordings if feasible would yield valuable information. 5) The wavefront velocity increases (e.g., in a logarithmic fashion) with the synaptic coupling strength; it drops sharply near the threshold for minimal AMPA. In concert with a gradually increasing dosage of AMPA-receptor antagonist, wavefront velocity could be measured either with recordings from multielectrode arrays along the slice (as used by Kim et al. 1995) or imaging as for 2. 6) When GABA<sub>A</sub> is blocked, the phase shift between neurons increases linearly with the distance between them; it varies with the system parameters such as  $g_{KL}$  of the RE cells. These measurements will be perhaps the most difficult to systematically quantify; the better temporal resolution of multielectrode recordings may be preferred over imaging.

We believe that 1–3 are general and may hold in thalamic slice preparations of other species that are capable of displaying spindle waves. Result 4 directly depends on a sufficiently slow wavefront propagation velocity. If the quantitative parametric dependencies of 5 and 6 are not confirmed by future experiments, modest revisions of the model will likely account for the discrepancies. However, if 1 and 4 are unconfirmed by ferret slice experiments, the model will require substantial revisions if it is to apply to this preparation.

#### APPENDIX A: MODEL EQUATIONS AND PARAMETERS

We use a Hodgkin-Huxley-like formulation for both the RE and TC cells. The intrinsic ionic currents were modeled on the basis of existing voltage-clamp data (see Golomb et al. 1994a). There are  $N_{\text{RE}}$  RE cells and  $N_{\text{TC}}$  TC cells; we assume  $N_{\text{RE}} = N_{\text{TC}} = N$ . We specify here our reference parameter set. They are used throughout the paper unless stated otherwise.

*RE cells*

## CURRENT BALANCE EQUATION.

$$C \frac{dV_i}{dt} = -I_{\text{Ca-T}}(V_i, h_i) - I_{\text{KL}}(V_i) - I_{\text{NL}}(V_i) \\ - I_{\text{AHP}}(V_i, m_{\text{AHP}}) - I_{\text{AMPA}}(V_i, \{s_{pj}\}) - I_{\text{GABA}_A}^{RR}(V_i, \{s_{aj}\}) \quad (\text{A1})$$

where  $C = 1 \mu\text{F}/\text{cm}^2$ .

## INTRINSIC CURRENTS.

$I_{\text{Ca-T}}$ .

$I_{\text{Ca-T}}(V, h) = g_{\text{Ca}} m_\infty^2(V) h(V - V_{\text{Ca}}) \quad (\text{A2})$

$\frac{dh}{dt} = [h_\infty(V) - h]/\tau_h(V) \quad (\text{A3})$

$m_\infty(V) = \{1 + \exp[-(V - \theta_m)/\sigma_m]\}^{-1} \quad (\text{A4})$

$h_\infty(V) = \{1 + \exp[-(V - \theta_h)/\sigma_h]\}^{-1} \quad (\text{A5})$

$\tau_h(V) = 23.8 + 119 \times \{1 + \exp[-(V - \theta_{ht})/\sigma_{ht}]\}^{-1} \quad (\text{A6})$

$g_{\text{Ca}} = 1.5 \text{ mS/cm}^2$ ,  $V_{\text{Ca}} = 120 \text{ mV}$ ,  $\theta_m = -52 \text{ mV}$ ,  $\sigma_m = 7.4 \text{ mV}$ ,  $\theta_h = -78 \text{ mV}$ ,  $\sigma_h = -5 \text{ mV}$ ,  $\theta_{ht} = -70 \text{ mV}$ ,  $\sigma_{ht} = -3 \text{ mV}$ . Gating kinetics have been adjusted to 36°C.

*Leak currents  $I_{\text{KL}}$ ,  $I_{\text{NL}}$ .*

$\text{Potassium leak current } I_{\text{KL}} = g_{\text{KL}}(V - V_{\text{K}}) \quad (\text{A7})$

$\text{Nonspecific leak current } I_{\text{NL}} = g_{\text{NL}}(V - V_{\text{NL}}) \quad (\text{A8})$

$g_{\text{KL}} = 0.025 \text{ mS/cm}^2$ ,  $V_{\text{K}} = -90 \text{ mV}$ ,  $g_{\text{NL}} = 0.01 \text{ mS/cm}^2$ ,  $V_{\text{NL}} = -72.5 \text{ mV}$ .

 $I_{\text{AHP}}$ .

$I_{\text{AHP}}(V, m_{\text{AHP}}) = g_{\text{AHP}} m_{\text{AHP}}(V - V_{\text{K}}) \quad (\text{A9})$

$\frac{d[\text{Ca}]}{dt} = -\nu I_{\text{Ca-T}} - \gamma [\text{Ca}] \quad (\text{A10})$

$\frac{dm_{\text{AHP}}}{dt} = \alpha [\text{Ca}] (1 - m_{\text{AHP}}) - \beta m_{\text{AHP}} \quad (\text{A11})$

$g_{\text{AHP}} = 0.1 \text{ mS/cm}^2$ ,  $\alpha = 0.02 \text{ ms}^{-1}$ ,  $\beta = 0.025 \text{ ms}^{-1}$ ,  $\nu = 0.01 \text{ cm}^2/(\text{ms} \times \mu\text{A})$ ,  $\gamma = 0.08 \text{ ms}^{-1}$ ;  $[\text{Ca}]$  is dimensionless.

## SYNAPTIC CURRENTS.

*AMPA current  $I_{\text{AMPA}}$  from TC to RE cells.*

$I_{\text{AMPA}}(V, \{s_{pj}\}) = g_{\text{AMPA}}(V - V_{\text{AMPA}}) \sum_{j=1}^N w_{\text{TR}}(i - j) s_{pj} \quad (\text{A12})$

$g_{\text{AMPA}} = 0.1 \text{ mS/cm}^2$ ,  $V_{\text{AMPA}} = 0 \text{ mV}$ . The gating variables  $\{s_{pj}\}$  depend on the membrane potential of the TC cells, and they are governed by (Eqs. A34 and A35), given below.

*GABA<sub>A</sub> current  $I_{\text{GABA}_A}^{RR}$  from RE to RE cells.*

$I_{\text{GABA}_A}^{RR}(V, \{s_{aj}\}) = g_{\text{GABA}_A}^{RR}(V - V_{\text{GABA}_A}) \sum_{j=1}^N w_{\text{RR}}(i - j) s_{aj} \quad (\text{A13})$

*GABA<sub>A</sub> gating variable.*

$\frac{ds_{aj}}{dt} = k_{fA} s_\infty(V_j) (1 - s_{aj}) - k_{rA} s_{aj} \quad (\text{A14})$

$s_\infty(V) = \{1 + \exp[-(V - \theta_s)/\sigma_s]\}^{-1}, \quad (\text{A15})$

where  $V_j$  is the presynaptic membrane potential.  $\theta_s = -40 \text{ mV}$ ,  $\sigma_s = 2 \text{ mV}$  (for both GABA<sub>A</sub> and GABA<sub>B</sub>),  $g_{\text{GABA}_A}^{RR} = 0.2 \text{ mS/cm}^2$ ,  $V_{\text{GABA}_A} = -75 \text{ mV}$ ,  $k_{fA} = 2.0 \text{ ms}^{-1}$ ,  $k_{rA} = 0.08 \text{ ms}^{-1}$ .

*GABA<sub>B</sub> gating variables.*

$\frac{dx_{bj}}{dt} = k_{fx} s_\infty(V_j) (1 - x_{bj}) - k_{rx} [1 - s_\infty(V_j)] x_{bj} \quad (\text{A16})$

$\frac{ds_{bj}}{dt} = k_{fb} x_{bj}^4 (1 - s_{bj}) - k_{rb} s_{bj} \quad (\text{A17})$

$k_{fx} = 0.02 \text{ ms}^{-1}$ ,  $k_{rx} = 0.05 \text{ ms}^{-1}$ ,  $k_{fb} = 0.03 \text{ ms}^{-1}$ ,  $k_{rb} = 0.01 \text{ ms}^{-1}$ . The variable  $x_{bj}$ , that corresponds to the activated G-protein level, grows with a rate  $k_{fx}$  during a burst; when the burst is not very wide, it is far from saturation, and the growth is linear in time. After a burst,  $x_{bj}$  decays exponentially. The nonlinear term  $x_{bj}^4$  in Eq. A17 causes  $s_{bj}$  to reach larger values for bursts of wide duration.

## ARCHITECTURE.

*TC-to-RE coupling.* By defining  $\Lambda_{\text{TR}} = N\lambda_{\text{TR}}$ , the maximal synaptic conductance from neuron  $j$  to neuron  $i$  is a function of  $(x_i - x_j)/\lambda_{\text{TR}} = (i - j)/\Lambda_{\text{TR}}$ , with  $x_i = i/N$  and  $x_j = j/N$ . The normalization condition (Eq. 6) implies that  $w_{\text{TR}}(x_i, x_j)$  is proportional to  $1/\Lambda_{\text{TR}}$  (and hence to  $1/N$ ) for large  $\Lambda_{\text{TR}}$ .

For an exponential footprint shape, the coupling coefficients  $w_{\text{TR}}$  are given by (with footprint length  $\Lambda_{\text{TR}} = 8$ )

$w_{\text{TR}}(j) = \frac{\exp(-|j|/\Lambda_{\text{TR}})}{\sum_{j=-N/2}^{N/2} \exp(-|j|/\Lambda_{\text{TR}})} \approx \tanh[1/(2\Lambda_{\text{TR}})] \exp(-|j|/\Lambda_{\text{TR}}) \quad (\text{A18})$

For the step footprint shape, they are

$w_{\text{TR}} = \begin{cases} \frac{1}{2\Lambda_{\text{TR}} + 1} & -\Lambda_{\text{TR}} \leq j \leq \Lambda_{\text{TR}} \\ 0 & \text{otherwise} \end{cases} \quad (\text{A19})$

The coupling coefficients  $w_{RR}(j)$  are given by Eq. A18 or Eq. A19 with footprint length  $\Lambda_{RR} (=8)$ .

*TC cells*

## CURRENT BALANCE EQUATION.

$C \frac{dV_i}{dt} = -I_{\text{Ca-T}}(V_i, h_i) - I_{\text{KL}}(V_i) - I_{\text{NL}}(V_i) - I_h(V_i, r_i) \\ - I_{\text{GABA}_A}(V_i, \{s_{aj}\}) - I_{\text{GABA}_B}(V_i, \{s_{bj}\}) \quad (\text{A20})$

where  $C = 1 \mu\text{F}/\text{cm}^2$ .

## INTRINSIC CURRENTS.

$I_{\text{Ca-T}}$ .

$I_{\text{Ca-T}}(V, h) = g_{\text{Ca}} m_\infty^2(V) h(V - V_{\text{Ca}}) \quad (\text{A21})$

$\frac{dh}{dt} = [h_\infty(V) - h]/\tau_h(V) \quad (\text{A22})$

$m_\infty(V) = \{1 + \exp[-(V - \theta_m)/\sigma_m]\}^{-1} \quad (\text{A23})$

$h_\infty(V) = \{1 + \exp[-(V - \theta_h)/\sigma_h]\}^{-1} \quad (\text{A24})$

$\tau_h(V) = 7.14 + 52.4 \times \{1 + \exp[-(V - \theta_{ht})/\sigma_{ht}]\}^{-1} \quad (\text{A25})$

$g_{\text{Ca}} = 2.0 \text{ mS/cm}^2$ ,  $V_{\text{Ca}} = 120 \text{ mV}$ ,  $\theta_m = -59 \text{ mV}$ ,  $\sigma_m = 6.2 \text{ mV}$ ,  $\theta_h = -81 \text{ mV}$ ,  $\sigma_h = -4.4 \text{ mV}$ ,  $\theta_{ht} = -74 \text{ mV}$ ,  $k_{ht} = -3 \text{ mV}$ . Gating kinetics have been adjusted to 36°C.

*Leak currents  $I_{\text{KL}}$ ,  $I_{\text{NL}}$ .*

$\text{Potassium leak current } I_{\text{KL}} = g_{\text{KL}}(V - V_{\text{K}}) \quad (\text{A26})$

$\text{Nonspecific leak current } I_{\text{NL}} = g_{\text{NL}}(V - V_{\text{NL}}) \quad (\text{A27})$

$g_{\text{KL}} = 0.02 \text{ mS/cm}^2$ ,  $V_{\text{K}} = -100 \text{ mV}$ ,  $g_{\text{NL}} = 0.01 \text{ mS/cm}^2$ ,  $V_{\text{NL}} = -55 \text{ mV}$ .

*Hyperpolarization-activated cation current (sag)  $I_h$ .*

$I_h(V, r) = g_h r(V - V_h) \quad (\text{A28})$

$\frac{dr}{dt} = [r_\infty(V) - r]/\tau_{\text{sag}}(V) \quad (\text{A29})$

$r_\infty(V) = \{1 + \exp[-(V - \theta_{\text{sag}})/\sigma_{\text{sag}}]\}^{-1} \quad (\text{A30})$

$$\tau_{\text{sag}}(V) = 20 + 1,000 / \{\exp[(V + 71.5)/14.2] + \exp[-(V + 89.0)/11.6]\} \quad (\text{A31})$$

$g_h = 0.04 \text{ mS/cm}^2$ ,  $V_h = -40.0 \text{ mV}$ ,  $\theta_{\text{sag}} = -75 \text{ mV}$ ,  $\sigma_{\text{sag}} = -5.5 \text{ mV}$ .

#### SYNAPTIC CURRENTS.

$GABA_A$  current  $I_{GABA_A}$  from RE to TC cells.

$$I_{GABA_A}(V, \{s_{Aj}\}) = g_{GABA_A}(V - V_{GABA_A}) \sum_{j=1}^N w_{RT}(i-j)s_{Aj} \quad (\text{A32})$$

$g_{GABA_A} = 0.1 \text{ mS/cm}^2$ ,  $V_{GABA_A} = -85 \text{ mV}$ ; see Eqs. A14–A15 for  $s_{Aj}$  kinetics.

$GABA_B$  current  $I_{GABA_B}$  from RE to TC cells.

$$I_{GABA_B}(V, \{s_{Bj}\}) = g_{GABA_B}(V - V_K) \sum_{j=1}^N w_{RT}(i-j)s_{Bj} \quad (\text{A33})$$

$g_{GABA_B} = 0.06 \text{ mS/cm}^2$ ; see Eqs. A15–A17 for  $s_{Bj}$  kinetics.

AMPA gating variable.

$$\frac{ds_{Pj}}{dt} = k_{fP}s_\infty(V)(1 - s_{Pj}) - k_{rP}s_{Pj} \quad (\text{A34})$$

$$s_\infty(V) = \{1 + \exp[-(V - \theta_s)/\sigma_s]\}^{-1} \quad (\text{A35})$$

$\theta_s = -40 \text{ mV}$ ,  $\sigma_s = 2 \text{ mV}$ ,  $k_{fP} = 2.0 \text{ ms}^{-1}$ ,  $k_{rP} = 0.1 \text{ ms}^{-1}$ .

ARCHITECTURE. The coupling coefficients  $w_{RT}(j)$  are given by Eq. A18 or Eq. A19 with footprint length  $\Lambda_{RT} (=8)$ .

#### APPENDIX B: RECRUITMENT LENGTH

The TC-to-RE recruitment length is defined to be the difference in spatial position between the rightmost (with the largest  $x$ ) RE cell that is bursting in a recruitment cycle and the rightmost TC cell that fired a burst at the previous cycle. The wavefront propagation during a cycle is equal to the sum of the TC-to-RE recruitment length  $\rho_{TR}$  and the RE-to-TC recruitment length  $\rho_{RT}$ , defined similarly (ignoring the irregularity near the wavefront). Here we present a simple analytic estimate of the TC-to-RE recruitment length. We assume that the number of neurons within the footprint length is large enough such that we can use continuum notation and approximate sums (Eqs. A12, A13, A32, and A33) by integrals. Subscripts are omitted. The RE-to-TC recruitment length is estimated in a similar way. We note that our estimation of recruitment length depends implicitly on the assumption of a lurching type wave; in each cycle, distinct groups of cells from different types are recruited. We would not use it to predict the wavefront velocity in other systems, such as continuous waves in excitatory networks (Miles et al. 1988; Traub et al. 1993).

Suppose that the wavefront position, measured in the TC population, has reached a point  $x_F$ . A quiescent RE cell located at a position  $x_F + x_o$  ( $x_o > 0$ ) will burst if the total excitation it receives exceeds the threshold  $\theta$ . We neglect temporal summation effects and assume that all the excitation arrives at the same time. The total excitation to the RE neuron from a bursting TC neuron at a position  $x_F + y$  is  $g \times s \times w(x_o - y)$ , where  $g$  is the total maximal synaptic conductance,  $s$  is a typical value for the synaptic variable, and  $w(x_o - y)$  is the synaptic footprint function. The total amount of excitation that the RE neuron receives should be larger than the threshold  $\theta$  in order to elicit a burst from that neuron

$$gs \int_{x_o}^{\infty} dy w(y) \geq \theta \quad (\text{B1})$$

The recruitment length  $\rho$  is given by the value of  $x_o$  for which the equality holds.

The step footprint shape with footprint length  $\lambda$  is given by the

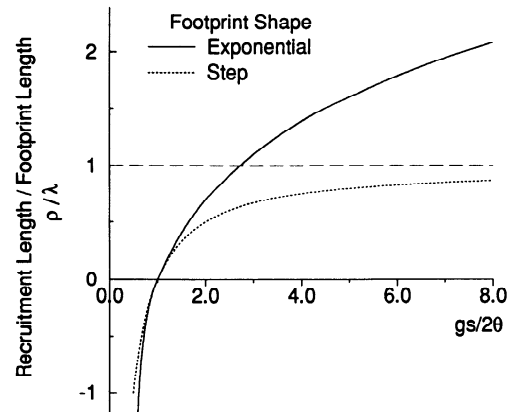


FIG. B1. Theoretical estimate for the dependence of the recruitment length on the synaptic coupling strength. The ratio between the recruitment and the footprint lengths ( $\rho/\lambda$ ) vs. the ratio  $gs/2\theta$  for exponential (—) and step (···) footprint shapes;  $g$  is a maximal synaptic conductance,  $s$  is a typical value of the synaptic gating variable, and  $\theta$  is the bursting threshold. With a step footprint shape, the recruitment length approaches the footprint length asymptotically with strong synaptic coupling strength (— · · ·). It is 0 for  $gs = 2\theta$ , negative for  $gs < 2\theta$ , and  $-\infty$  for  $gs < \theta$ .

continuous form of Eq. A19:  $w(y) = 1/2\lambda$  if  $-\lambda \leq y \leq \lambda$  and it is zero otherwise. Substituting it into Eq. B1, one obtains

$$\rho = \begin{cases} \lambda \left(1 - \frac{2\theta}{gs}\right) & gs \geq 2\theta \\ -\infty & gs < \theta \end{cases} \quad (\text{B2})$$

Negative  $\rho$  means that the RE neuron with the largest  $x$  that bursts at this recruitment cycle is located behind (left of) the rightmost TC neuron that had most recently burst;  $\rho = -\infty$  means that no RE cell will burst in this cycle, and the system goes to rest. For an exponential coupling,  $w(y) = 1/(2\lambda) \exp(-|y|/\lambda)$ . The recruitment length is

$$\rho = \begin{cases} \lambda \ln\left(\frac{gs}{2\theta}\right) & gs \geq 2\theta \\ \lambda \ln\left(2 - \frac{2\theta}{gs}\right) & \theta \leq gs \leq 2\theta \\ -\infty & gs < \theta \end{cases} \quad (\text{B3})$$

The ratios between the recruitment and the footprint lengths are shown in Fig. B1.

For all symmetric footprint shapes, the recruitment length is positive only if  $gs > 2\theta$ . The total amount of excitation that a neuron just near the wavefront receives is  $gs/2$ , and this level must be larger than the threshold for the wavefront to propagate. Similarly, cells are recruited at all only if  $gs > \theta$ . It is easily seen that near the critical conductance for positive recruitment length ( $gs \gtrsim 2\theta$ ) the recruitment length is

$$\rho = \frac{1 - 2\theta/gs}{2w(0)} \quad (\text{B4})$$

for any footprint shape. For both the step and exponential footprint shapes,  $w(0) = 1/2\lambda$ , and therefore  $\rho = \lambda(1 - 2\theta/gs)$ . This formula is identical to Eq. B2 and coincides with Eq. B3 for  $gs$  just above the critical conductance. For strong connectivity ( $gs \gg 2\theta$ ), the recruitment length  $\rho$  approaches the footprint length  $\lambda$  for a step footprint shape and grows logarithmically for an exponential footprint shape.

APPENDIX C: PHASE SHIFT: DECAY AND NORMALIZATION

The phase shift occurs as a transient phenomenon. After the wavefront has propagated across the slice, the phase shift decreases asymptotically with time to a near-zero value. The dynamical explanation of this phenomena is the following. If the boundary conditions were periodic, instead of open, the fully synchronized state would exist and be stable. However, transients decay exponentially with time. It can be shown analytically that for symmetric coupling, as in our study, the decay time scales like the square of the ratio between the slice length and the typical footprint length and can be very long if both  $\lambda_{RT}$  and  $\lambda_{TR}$  are much smaller than one. In our case the boundary conditions are open, but we have shown numerically that except in a regime near the edges, the phase shift decays exponentially in time with the same scaling law (data not shown). Because the decay time may be much larger than the time period of the spindle episodes, phase shifts can in principle be detected in experiments.

To compare the phase shift  $\phi$  in our model and in the in vitro experiments, the phase shift should be normalized. In the model, it depends on the footprint lengths ( $\lambda_{RT}$  and  $\lambda_{TR}$ ). For instance, if  $\lambda_{RT}$  and  $\lambda_{TR}$  are increased by a factor of 2, the wavefront velocity  $v_F$  will be doubled (Fig. 9), whereas the phase shift  $\phi$  will be reduced to one-half of its original value; the product  $\phi v_F$  remains constant. Here we show that the dimensionless quantity  $\mu = \phi v_F$  should be used when a comparison between the model and experimental results is made.

The slice length, phase shift, wavefront velocity, and time period in the experiment are  $L_E$ ,  $\phi_E$ ,  $v_{F,E}$ , and  $T_E$ , respectively. The corresponding values for the model are  $L_M$ ,  $\phi_M$ ,  $v_{F,M}$ , and  $T_M$ . Suppose we know  $L_E$ ,  $v_{F,E}$ , and  $T_E$ , and we want to predict  $\phi_E$  based on these values and our model. In the experiment, the number of cycles needed for the wavefront to propagate across the whole slice is  $N_E = L_E/(v_{F,E}T_E)$ , and in the model it is  $N_M = L_M/(v_{F,M}T_M)$ . The phase shift predicted by the model for the same number of cycles  $N_E$  is, assuming  $T_E = T_M$

$$\phi_E^{\text{predicted}} = \frac{N_E}{N_M} \phi_M = \frac{\phi_M V_{F,M}/L_M}{V_{F,E}/L_E} \quad (C1)$$

In this formula for the predicted experimental phase shift, the only quantity that comes from the model is  $\mu = \phi_M V_{F,M}/L_M$ . Because the model slice length is normalized to 1, we get the dimensionless quantity  $\mu = \phi_M V_{F,M}$ .

We are grateful to C. Asanuma, T. Bal, D. Contreras, A. Destexhe, B. Ermentrout, D. Hansel, D. McCormick, B. Softky, and M. Steriade for helpful discussions. We acknowledge computer time provided by the National Cancer Institute Biomedical Supercomputing Center.

Present addresses: D. Golomb, Zlotowski Center for Neuroscience and Dept. of Physiology, Faculty of Health Sciences, P.O.B. 653, Ben-Gurion University of the Negev, Beer-Sheva 84105, Israel; X.-J. Wang, Center for Complex Systems and Physics Dept., Brandeis University, Waltham, MA 02254.

X.-J. Wang was supported by National Science Foundation Grant IBN-9409202, and by an Alfred P. Sloan Fellowship.

Address for reprint requests: J. Rinzel, Mathematical Research Branch, NIDDK, National Institutes of Health, 9190 Wisconsin Ave., Suite 350, Bethesda, MD 20814.

Received 11 April 1995; accepted in final form 11 September 1995.

## REFERENCES

- ANDERSEN, P. AND ANDERSSON, S. A. *Physiological Basis of the Alpha Rhythm*. New York: Appleton-Century-Crofts, 1968.
- ANDERSEN, P., ANDERSSON, S. A., AND LOMO, T. Patterns of spontaneous rhythmic activity within various thalamic nuclei. *Nature Lond.* 211: 888–889, 1966.
- ANDERSON, P. W. AND STEIN, D. L. Broken symmetry, emergent properties, dissipative structures, life and its origin: are they related? In: *Self-Organizing Systems: The Emergence of Order*, edited by F. E. Yates. New York: Plenum, 1984.
- BAL., T., VON KROSIKG, M., AND MCCORMICK, D. A. Oscillations in thalamocortical networks. *Euromedicine 94*, Montpellier, Le Corum, 1994.
- BAL., T., VON KROSIKG, M., AND MCCORMICK, D. A. Synaptic and membrane mechanisms underlying synchronized oscillations in the ferret LGNd in vitro. *J. Physiol. Lond.* 483: 641–663, 1995a.
- BAL., T., VON KROSIKG, M., AND MCCORMICK, D. A. Role of the ferret perigeniculate nucleus in the generation of synchronized oscillations in vitro. *J. Physiol. Lond.* 483: 665–685, 1995b.
- BARKAI, E., KANTER, I., AND SOMPOLINSKY, H. Properties of sparsely connected neural networks. *Physiol. Rev. A* 41: 590–597, 1990.
- BLOOMFIELD, S. A., HAMOS, J. E., AND SHERMAN, S. M. Passive cable properties and morphological correlates of neurons in the lateral geniculate nucleus of the cat. *J. Physiol. Lond.* 383: 653–692, 1987.
- BUZSÁKI, G. The thalamic clock: emergent network properties. *Neuroscience* 41: 351–364, 1991.
- CHERVIN, R. D., PIERCE, P. A., AND CONNORS, B. W. Periodicity and directionality in the propagation of epileptiform discharges across neocortex. *J. Neurophysiol.* 60: 1695–1713, 1988.
- CONTRERAS, D., CURRÓ DOSSI, R., AND STERIADE, M. Electrophysiological properties of cat reticular thalamic neurones in vivo. *J. Physiol. Lond.* 470: 273–294, 1993.
- CUCCHIARO, J. B., UHLRICH, D. J., AND SHERMAN, S. M. Electron-microscopic analysis of synaptic input from the perigeniculate nucleus to the A-laminae of the lateral geniculate nucleus in cats. *J. Comp. Neurol.* 310: 316–336, 1991.
- DESCHIÈNES, M., PARADIS, M., ROY, J. P., AND STERIADE, M. Electrophysiology of neurons of lateral thalamic nuclei in rat: resting properties and burst discharges. *J. Neurophysiol.* 51: 1196–1219, 1984.
- DESTEXHE, A., CONTRERAS, D., SEJNOWSKI, T. J., AND STERIADE, M. A model of spindle rhythmicity in the isolated thalamic reticular nucleus. *J. Neurophysiol.* 72: 803–818, 1994a.
- DESTEXHE, A., CONTRERAS, D., SEJNOWSKI, T. J., AND STERIADE, M. Modeling the control of reticular thalamic oscillations by neuromodulators. *NeuroReport* 5: 2217–2220, 1994b.
- DESTEXHE, A., MAINEN, Z. F., AND SEJNOWSKI, T. J. Synthesis of models for excitable membranes, synaptic transmission and neuromodulation using a common kinetic formalism. *J. Comput. Neurosci.* 1: 195–230, 1994c.
- DESTEXHE, A., MCCORMICK, D. A., AND SEJNOWSKI, T. J. A model for 8–10 Hz spindling in interconnected thalamic relay and reticularis neurons. *Biophys. J.* 65: 2473–2477, 1993.
- DESTEXHE, A. AND SEJNOWSKI, T. J. Spill-over of GABA and G-protein cooperativity account for differences between inhibitory responses in the hippocampus and thalamus. *Proc. Natl. Acad. Sci. USA* 92: 9515–9519, 1995.
- ERMENTROUT, G. B. AND MCLEOD, J. B. Existence and uniqueness of travelling waves for a neural network. *Proc. R. Soc. Edinburgh* 123A: 461–478, 1993.
- FRIEDLANDER, M. J., LIN, C.-S., STANFORD, L. R., AND SHERMAN, S. M. Morphology of functionally identified neurons in lateral geniculate nucleus of the cat. *J. Neurophysiol.* 46: 80–129, 1981.
- GOLOMB, D. AND RINZEL, J. Dynamics of globally coupled inhibitory neurons with heterogeneity. *Physiol. Rev.* 74: 4810–4814, 1993.
- GOLOMB, D. AND RINZEL, J. Clustering in globally coupled inhibitory neurons. *Physica D* 72: 259–282, 1994.
- GOLOMB, D., WANG, X.-J., AND RINZEL, J. Synchronization properties of spindle oscillations in a thalamic reticular nucleus model. *J. Neurophysiol.* 72: 1109–1126, 1994a.
- GOLOMB, D., WANG, X.-J., AND RINZEL, J. Subharmonic bursting of an RE-TC thalamic network during spindle oscillations. *Soc. Neurosci. Abstr.* 20: 118, 1994b.
- GOLOMB, D., WANG, X.-J., AND RINZEL, J. Partial and full synchrony of thalamic spindle oscillations. In: *The Neurobiology of Computation*, edited by J. Bower. Boston, MA: Kluwer, 1995, p. 215–220.
- GRAY, C. M. Synchronous oscillations in neuronal systems: mechanisms and functions. *J. Comput. Neurosci.* 1: 11–38, 1994.
- HANSEL, D. AND SOMPOLINSKY, H. Chaos and synchrony in a model of a hypercolumn in visual cortex. *J. Comput. Neurosci.* In press.
- HARRIS, R. M. Axon collaterals in the thalamic reticular nucleus from thalamocortical neurons of the rat ventrobasal thalamus. *J. Comp. Neurol.* 258: 397–406, 1987.

- HODGKIN, A. L. AND HUXLEY, A. F. A quantitative description of membrane current and its application to conduction and excitation in nerve. *J. Physiol. Lond.* 117: 500–544, 1952.
- HUGUENARD, J. R. AND PRINCE, D. A. A novel T-type current underlies prolonged  $\text{Ca}^{2+}$ -dependent burst firing in GABAergic neurons of rat thalamic reticular nucleus. *J. Neurosci.* 12: 3804–3817, 1992.
- HUGUENARD, J. R. AND PRINCE, D. A. Clonazepam suppresses  $\text{GABA}_B$ -mediated inhibition in thalamic relay neurons through effects in nucleus reticularis. *J. Neurophysiol.* 71: 2576–2581, 1994.
- IDE, L. S. The fine structure of the perigeniculate nucleus in the cat. *J. Comp. Neurol.* 210: 317–334, 1982.
- IDIART, M. A. P. AND ABBOTT, L. F. Propagation of excitation in neural network models. *Network* 4: 285–294, 1993.
- JAHNSEN, H. AND LLINÁS, R. R. Electrophysiological properties of guinea-pig thalamic neurons: an *in vitro* study. *J. Physiol. Lond.* 349: 205–226, 1984a.
- JAHNSEN, H. AND LLINÁS, R. R. Ionic basis for the electroresponsiveness and oscillatory properties of guinea-pig thalamic neurons *in vitro*. *J. Physiol. Lond.* 349: 227–247, 1984b.
- KIM, U., BAL, T., AND MCCORMICK, D. A. Spindle waves are propagating synchronized oscillations in the ferret LGNd *in vitro*. *J. Neurophysiol.* 74: 1301–1323, 1995.
- KOCH, C. AND SEGEV, I. *Methods in Neuronal Modeling*. Cambridge, MA: MIT Press, 1989.
- KOPELL, N. AND LEMASSON, G. Rhythmogenesis, amplitude modulation and multiplexing in a cortical architecture. *Proc. Natl. Acad. Sci. USA* 91: 10586–10590, 1994.
- LEE, K., BAL, T., AND MCCORMICK, D. A. Waking up the sleeping slice: neuromodulation of spindle waves *in vitro*. *Soc. Neurosci. Abstr.* 20: 133, 1994.
- LEE, K. H. AND MCCORMICK, D. A. Acetylcholine excites GABAergic neurons of the ferret perigeniculate nucleus through nicotinic receptors. *J. Neurophysiol.* 73: 2123–2128, 1995.
- LERESCHE, N., LIGHTowler, S., SOLTESZ, I., JASSIK-GERSCHENFELD, D., AND CRUNELLI, V. Low-frequency oscillatory activities intrinsic to cat and rat thalamocortical cells. *J. Physiol. Lond.* 441: 155–174, 1991.
- MARKRAM, H. AND SAKMANN, B. Effects of action potentials propagating back into dendrites on synaptic transmission between neighboring layer V pyramidal neurons. *IBRO Abstr., 4th IBRO World Congr. Neurosci.* S17.5, 1995.
- MCCORMICK, D. A. Neurotransmitter actions in the thalamus and cerebral cortex and their role in neuromodulation of thalamocortical activity. *Prog. Neurobiol.* 39: 337–388, 1992.
- MCCORMICK, D. A. AND BAL, T. Sensory gating mechanisms of the thalamus. *Curr. Opin. Neurobiol.* 4: 550–556, 1994.
- MCCORMICK, D. A. AND HUGUENARD, J. R. A model of the electrophysiological properties of thalamocortical relay neurons. *J. Neurophysiol.* 68: 1384–1400, 1992.
- MCCORMICK, D. A. AND PAPE, H.-C. Properties of a hyperpolarization activated cation current and its role in rhythmic oscillation in thalamic relay neurons. *J. Physiol. Lond.* 431: 291–318, 1990.
- MCCORMICK, D. A. AND WANG, Z. Serotonin and noradrenaline excite GABAergic neurones of the guinea-pig and cat nucleus reticularis thalami. *J. Physiol. Lond.* 442: 235–255, 1991.
- MILES, R., TRAUB, R. D., AND WONG, K. S. Spread of synchronous firing in longitudinal slices from the CA3 region of the hippocampus. *J. Neurophysiol.* 60: 1481–1496, 1988.
- MODY, I., DE KONINCK, Y., OTIS, T. S., AND SOLTESZ, I. Bridging the cleft at GABA synapses in the brain. *Trends Neurosci.* 17: 517–525, 1994.
- MORISON, R. S. AND BASSETT, D. L. Electrical activity of the thalamus and basal ganglia in decorticated cats. *J. Neurophysiol.* 8: 309–314, 1945.
- OTIS, T. S., DE KONINCK, Y. D., AND MODY, I. Characterization of synaptically elicited  $\text{GABA}_B$  responses using patch-clamp recordings in rat hippocampal slices. *J. Physiol. Lond.* 463: 391–407, 1993.
- PAPE, H.-C., BUDDE, T., MAGER, R., AND KISVÁRDY, Z. F. Prevention of  $\text{Ca}^{2+}$ -mediated action potentials in GABAergic local circuit neurones of rat thalamus by a transient  $\text{K}^+$  current. *J. Physiol. Lond.* 478: 403–422, 1994.
- PERKEL, D. H. AND MULLONEY, B. Motor pattern production in reciprocally inhibitory neurons exhibiting postinhibitory rebound. *Science Wash. DC* 185: 181–183, 1974.
- PINAULT, D., BOURASSA, J., AND DESCHÈNES, M. The axonal arborization of single thalamic reticular neurons in the somatosensory thalamus of the rat. *Eur. J. Neurosci.* 7: 31–40, 1995.
- PRESS, W. H., FLANNERY, B. P., TEUKOLSKY, S. A., AND VETTERLING, W. T. *Numerical Recipes. The Art of Scientific Computing*. Cambridge, UK: Cambridge Univ. Press, 1989.
- RALL, W. Distinguishing theoretical synaptic potentials computed for different some-dendritic distribution of synaptic input. *J. Neurophysiol.* 30: 1138–1168, 1967.
- SHERMAN, S. M. AND KOCH, C. Thalamus. In: *The Synaptic Organization of the Brain*, edited by G. M. Shepherd. Oxford, UK: Oxford Univ. Press, 1990.
- STERIADE, M., CONTRERAS, D., AND AMZICA, F. Synchronized sleep oscillations and their paroxysmal developments. *Trends Neurosci.* 17: 199–208, 1994.
- STERIADE, M. AND DESCHÈNES, M. The thalamus as a neuronal oscillator. *Brain Res. Rev.* 8: 1–63, 1984.
- STERIADE, M., DESCHÈNES, M., DOMICH, L., AND MULLE, C. Abolition of spindle oscillations in thalamic neurons disconnected from nucleus reticularis thalami. *J. Neurophysiol.* 54: 1473–1497, 1985.
- STERIADE, M., DOMICH, L., OAKSON, G., AND DESCHÈNES, M. The differentiated reticularis thalami nucleus generates spindle rhythmicity. *J. Neurophysiol.* 57: 260–273, 1987.
- STERIADE, M., JONES, E. G., AND LLINÁS, R. R. *Thalamic Oscillations and Signaling*. New York: Wiley, 1990.
- STERIADE, M., MCCORMICK, D. A., AND SEJNOWSKI, T. J. Thalamocortical oscillations in the sleeping and aroused brain. *Science Wash. DC* 262: 679–685, 1993.
- STUART, G. J. AND SAKMANN, B. Active propagation of somatic action potentials into neocortical pyramidal cell dendrites. *Nature Lond.* 367: 69–72, 1994.
- TRAUB, R. D., JEFFERYS, J. G. R., AND MILES, R. Analysis of the propagation of disinhibition-induced after-discharges along the guinea-pig hippocampal slice *in vitro*. *J. Physiol. Lond.* 472: 267–287, 1993.
- UHLRICH, D. J., CUCCIARO, J. B., HUMPHREY, A. L., AND SHERMAN, S. M. Morphology and axonal projection patterns of individual neurons in the cat perigeniculate nucleus. *J. Neurophysiol.* 65: 1528–1541, 1991.
- VON KROSIKG, M., BAL, T., AND MCCORMICK, D. A. Cellular mechanisms of a synchronized oscillation in the thalamus. *Science Wash. DC* 261: 361–364, 1993.
- WANG, X.-J. Multiple dynamical modes of thalamic relay neurons: rhythmic bursting and intermittent phase-locking. *Neuroscience* 59: 21–31, 1994.
- WANG, X.-J., GOLOMB, D., AND RINZEL, J. Emergent spindle oscillations and intermittent burst firing in a thalamic model: specific neuronal mechanisms. *Proc. Natl. Acad. Sci. USA* 92: 5577–5581, 1995.
- WANG, X.-J. AND RINZEL, J. Alternating and synchronous rhythms in reciprocally inhibitory model neurons. *Neural Comp.* 4: 84–97, 1992.
- WANG, X.-J. AND RINZEL, J. Spindle rhythmicity in the reticularis thalami nucleus: synchronization among mutually inhibitory neurons. *Neuroscience* 53: 899–904, 1993.
- WANG, X.-J., RINZEL, J., AND ROGAWSKI, M. A. A model of the T-type calcium current and the low threshold spike in thalamic neurons. *J. Neurophysiol.* 66: 839–850, 1991.
- WARREN, R. A., AGMON, A., AND JONES, E. G. Oscillatory synaptic interactions between ventroposterior and reticular neurons in mouse thalamus *in vitro*. *J. Neurophysiol.* 72: 1993–2003, 1994.